Biomimetic Shark Skin Design: The Bristling Effect of Denticles

by

S.R.R. Baeten

To obtain the degree of Master of Science at the Delft University of Technology,
to be defended publicly on 28-11-24

Studentnumber:	4594266
Thesis committee:	Dr. A. Sakes, TU Delft
	Dr. J. Jovanova, TU Delft
	Dr. A. Laskari, TU Delft

TU Delft

Abstract

This thesis explores the fabrication of biomimetic shark skin, focusing on actively controlling the bristling effect of denticles, inspired by the passive bristling effect observed in the skin of Shortfin Mako sharks. By examining the natural structure and functionality of shark skin, the research aims to replicate its unique properties using innovative fabrication techniques. A review of previous methods for replicating shark skin structures led to the selection of an indirect fabrication approach, driven by the necessity to integrate an actuation mechanism. Drawing inspiration from soft robotics, the study identified Nitinol, a shape memory alloy, as the optimal material for actuation due to its significant force exertion and seamless integration into the silicone shark skin. Experiments were conducted in a water tank, testing various configurations of biomimetic shark skin to evaluate the performance of the integrated actuation mechanism. The initial findings demonstrated that Nitinol wire actuation within a silicone matrix effectively mimics the bristling mechanism, even in aquatic environments, showing sufficient strength to counteract water flow. While this research successfully demonstrated the feasibility of integrating actuation mechanisms into biomimetic shark skin, further studies are necessary to optimize the design for practical applications.

Contents

1 Introduction **3**
- 1.1 Motivation . . . 3
- 1.2 Thesis objective and scope . . . 5

2 Skin Characteristics of the Shortfin Mako Shark **6**
- 2.1 Morphology and Kinematics of the denticles . . . 6
- 2.2 Denticle pattern . . . 9
- 2.3 Hydrodynamics and flow analysis . . . 11

3 Methods and Materials **15**
- 3.1 Design and prototyping . . . 15
  - 3.1.1 Biomimetic replication . . . 15
  - 3.1.2 Denticle design . . . 16
  - 3.1.3 Denticle bristling mechanism . . . 18
  - 3.1.4 Actuation of denticle bristling mechanism . . . 20
  - 3.1.5 Bristling mechanism design parameters . . . 22
    - 3.1.5.1 Global bristling mechanism and body curvature . . . 24
    - 3.1.5.2 Local bristling mechanism . . . 26
- 3.2 Shape Memory Alloy: Nitinol . . . 27
  - 3.2.1 NiTi wire . . . 27
  - 3.2.2 Temperature development in the Nitinol wire . . . 28
  - 3.2.3 Characterization of the actuation mechanism . . . 30
- 3.3 Fabrication process . . . 31

4 Test setup Analysis **32**
- 4.1 Test set-up . . . 32
- 4.2 Different Test Configurations . . . 34
- 4.3 Results . . . 36

5 Discussion **39**
- 5.1 Limitations . . . 40
- 5.2 Recommendations . . . 40

6 Conclusion **41**

A Appendix A: Literature study **45**

1 Introduction

1.1 Motivation

Sharks have evolved over millions of years to optimise the hydrodynamic efficiency of their skin, allowing sharks to navigate through the water with minimal drag. The skin is decorated with tiny denticles in the dermis, often described as tooth-like structures, that extend from a flexible epidermis. These denticles come in different sizes and shapes, depending on their location on the body and typically have a width of 0.1 mm to 1 mm (Lloyd et al., 2021). The denticles have a longitudinally oriented pattern of riblets arranged in rows in the same direction as the water flow, as shown in Figure 1 (Bushnell & Moore, 1991; Dean & Bhushan, 2010). One of the functions of the denticles is disrupting the boundary layer of water next to the skin, regulating flow separation around the body and, as a result, reducing resistance during swimming (Díez et al., 2015).
By mimicking these properties, biomimetic shark skin is intended to improve the efficiency of underwater vehicles, aeroplanes and other structures, leading to reduced energy consumption and increased maneuverability.

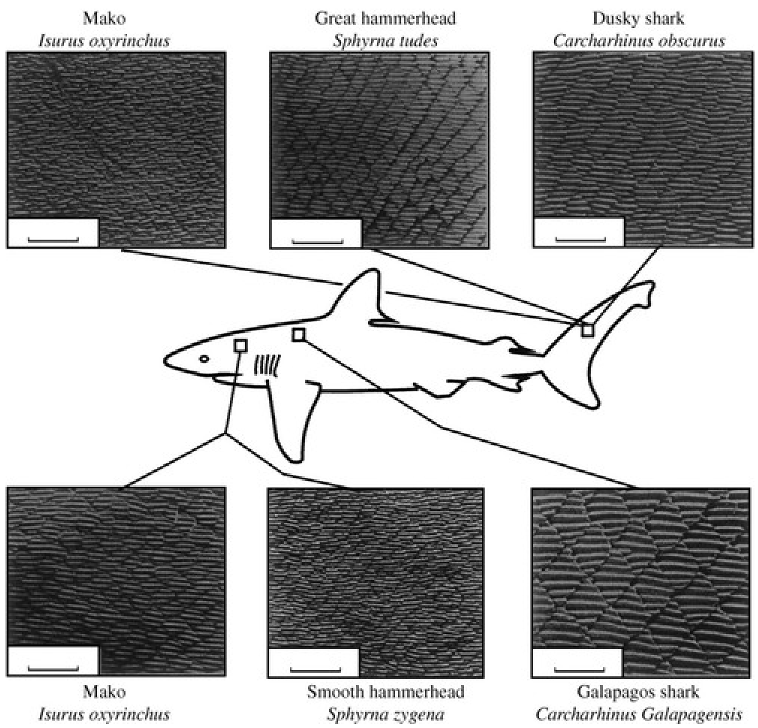

Figure 1: Denticle shapes, sizes and patterns among different species of sharks and location on the body (Dean & Bhushan, 2010).

Researchers have already aimed to simplify denticle morphology, which are illustrated in Figure 2, to create cost-effective and feasible riblet structures for mass applications. For instance, in the aircraft industry, a reduction in fuel consumption of up to 3 % has been achieved by applying a riblet structure on 70 % of the surface area (Pu et al., 2016). For pipe flow engineering, riblet-structured surfaces have been employed for drag reduction in pipe flow and have proven at least a 5 % resistance reduction (Pu et al., 2016).

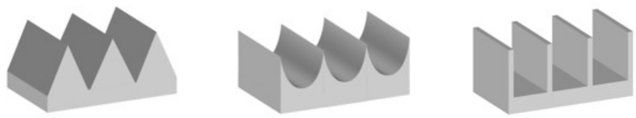

(a) Sawtooth (b) Scalloped (c) Blade

Figure 2: Common riblet geometries

However, researchers currently focus increasingly on developing the intricate microstructures of shark skin to achieve greater drag reduction.
The Shortfin Mako shark (*Isurus oxyrinchus*) is a widely studied species renowned for being one of the fastest swimmers among sharks. This impressive speed is attributed not only to its streamlined profile but also to a unique adaptation known as bristling. The bristling effect of the dermal denticles on the skin, illustrated in Figure 3, allows the Mako shark to passively control the separation of water currents along its body. By minimizing flow separation, the shark significantly enhances its hydrodynamic performance (A. W. Lang et al., 2014). This adaptation reduces drag and increases swimming efficiency, enabling the Mako shark to achieve remarkable speeds in the water.

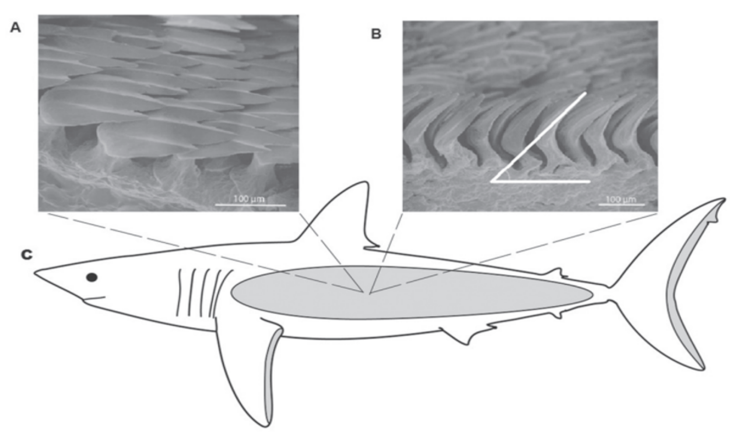

Figure 3: Bristling effect of the Shortfin Mako shark

Although the bristling mechanism of the dermal denticles of the Shortfin Mako shark has been studied extensively, its application in biomimetic skin designs remains limited. Despite the well-documented benefits of these denticles in reducing drag and enhancing thrust, translating these complex structures into practical, synthetic materials has proven challenging.

Appendix A provides a literature review titled Characterization of Shark Skin Properties and Biomimetic Replication. This review investigates the unique drag-reducing properties of shark skin, focusing on the influence of dermal denticles on fluid dynamics, and explores potential industrial applications for reducing friction in vessels and aircraft. It highlights various fabrication techniques, including 3D printing, and suggests future research on biomimetic shark skin to further enhance drag reduction and thrust.
This review examines the bristling effect observed in the Shortfin Mako shark, discussing the potential advantages this effect could offer if integrated into biomimetic shark skin designs. Graybill and Xu (2024) reviews recent research on manufacturing techniques and drag reduction studies of shark skin-inspired surfaces, suggesting that future developments should incorporate a wider variety of denticle geometries and additional factors such as bristling.
The ability to actively control the bristling angle of the denticles on biomimetic skin allows for real-time adaptation to changing flow conditions. Studying and replicating the adaptive features of shark skin could potentially transform various industries by offering innovative solutions for reducing drag and enhancing efficiency in both aquatic and aerodynamic applications.

1.2 Thesis objective and scope

The objective of this thesis is to design, fabricate, and evaluate a biomimetic shark skin inspired by the denticles found on Shortfin Mako sharks.
The focus is on developing a system that enables active control over the bristling effect of these denticles by investigating actuation mechanisms to achieve dynamic control over the surface. By actively controlling the bristling effect, surfaces can dynamically adjust their properties to suit different conditions. This could potentially transform areas such as fluid dynamics, where texture-changing surfaces could optimise flow, reduce flow separation and improve fuel efficiency in vehicles such as planes, cars and boats. By implementing a controlled experimental setup with water flow conditions, the actuation mechanism as well as the hydrodynamic performance of the biomimetic shark skin will be assessed. This research aims to contribute to the advancement of biomimetic materials and systems by emulating the unique adaptive properties of shark skin, particularly the Shortfin Mako shark, with the goal of enhancing hydrodynamic performance and control in underwater applications.

2 Skin Characteristics of the Shortfin Mako Shark

2.1 Morphology and Kinematics of the denticles

The dimensions and shape of the denticles vary depending on the shark species and their anatomical placement (A. Lang et al., 2008). According to Zhang et al. (2022), who conducted research on the Shortfin Mako shark (*Isurus oxyrinchus*), the length of the denticles ranges between 105 ± 7 μm and 286 ± 25 μm and the width of the denticles between 87 ± 4 μm and 255 ± 22 μm. The length-to-width ratio ranged from 1.02 to 1.45. In addition, Díez et al. (2015) found that the average height is between 90–110 μm, which includes the height of the peduncle (the base of the denticle) that connects the crown to the skin.
Several studies have examined the morphological characteristics of the Shortfin Mako shark in different body regions. Understanding this morphology is crucial for design inspiration.
Patricia et al. (2019) has conducted extensive research on the differences in morphology of the Mako shark's dorsal fin shown in Figure 4a. Understanding the microscopic dimensions of dermal denticles on the dorsal fin of the Shortfin Mako shark is essential for understanding its hydrodynamic behavior because the dorsal fin serves as a stabilizer that influences the shark's trajectory by minimizing drag and facilitating changes in swimming direction. The dorsal fin is divided into three different groups determined based on the length-width ratio. The three groups are rounded (L/W < 1.31) , semi rounded (1.31 > L/W < 1.35) , and long (L/W > 1.35) and dimensions are listed in Table 1.

Table 1: Morphological Measurements of Dorsal fin denticles

	Rounded (n = 46)	Semi-rounded (n = 38)	Long (n = 37)
Length (μm)	171.58 (20.36)	154.86 (15.32)	148.24 (9.36)
Width (μm)	131.38 (17.50)	116.15 (10.77)	109.93 (6.44)
L/W	1.31 (0.10)	1.33 (0.11)	1.35 (0.11)
LCW (μm)	41.05 (6.91)	36.80 (3.52)	34.93 (2.59)
RCW (μm)	41.17 (6.92)	36.76 (3.88)	33.78 (2.12)
DV (μm)	7.71 (1.51)	7.94 (1.99)	7.64 (1.79)
L/DV	17.58 (4.39)	15.79 (4.61)	15.67 (3.91)
W/DV	13.42 (3.44)	11.88 (3.67)	11.52 (2.90)
DV/LCW	0.191 (0.06)	0.211 (0.07)	0.208 (0.07)
DV/RCW	0.189 (0.06)	0.211 (0.07)	0.216 (0.08)

Note: L: Length of the denticle, W: Width of the denticle (when viewed from above), LCW: Left Crest Width, RCW: Right Crest Width, DV: Depth of the Valley.

Patricia et al. (2019) evaluated the three denticle shapes (round, semi-round and long) using a Computational Fluid Dynamics (CFD) model, considering two distinct angles of attack, 9.5 and 26.5 degrees and water velocities of 2 m/s and 5 m/s. At a speed of 2 m/s, the rounded morphology exhibits the highest drag coefficient of the three morphologies. However, this apparent disadvantage in drag coefficient is compensated by its consistent performance across different inclinations. This means that the rounded morphology maintains reliable hydrodynamic efficiency over a wide range of flow conditions. In contrast, the semi-rounded and long morphologies show remarkable increase in drag coefficients at higher inclination angles. As a

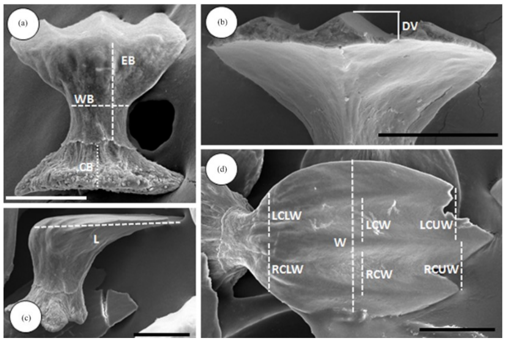

(a) Micrographs of a single denticle obtained through scanning electron microscopy (SEM) (Patricia et al., 2019). CB: Covered Base, EB: Exposed Base, WB: Width of the Base, DV: Depth of the Valley, L: Length of the dermal denticle, W: Width of the denticle (when viewed from above), LCW: Left Crest Width, RCW: Right Crest Width, LCUW: Left Crest Upper Width, RCUW: Right Crest Upper Width, LCLW: Left Crest Lower Width, RCLW: Right Crest Lower.

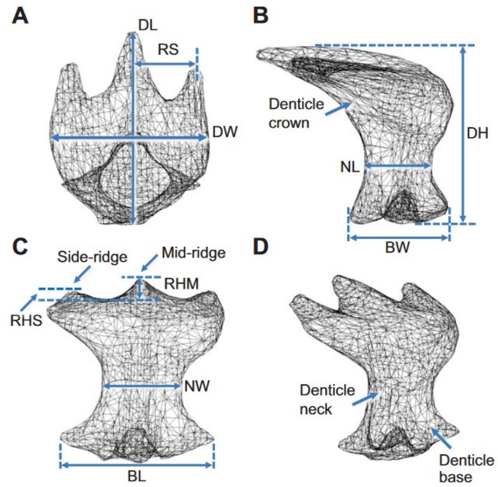

(b) 3D constructed single denticle of the Mako shark at the mid-trunk region (Wen et al., 2014).

Figure 4: Single shark denticle

result, it is suggested by Patricia et al. (2019) that the rounded denticles perform better than the semi-rounded denticles since they exhibit a more constant drag coefficient at different angles of attack and at different velocities of water.

Wen et al. (2014) and Zhang et al. (2022) have both performed morphological studies on flank-positioned denticles and the dimensions are shown in Table 2 and 3 respectively. Figure 4b illustrates a 3D reconstruction of a single denticle located on the flank. The flank of the Mako shark is a crucial part of the body because this is where the most flexible denticles are located. This suggests that the bristling effect plays a crucial role along the shark's flanks, reducing drag during high-speed swimming. The flexibility of the denticles is influenced by two factors: a shorter base relative to the crown length and changes in the length of the front and back of the base of the denticle. The denticles on the flank have a greater ratio of crown length to base length, with a significantly shorter base. Firmly anchored denticles have an evenly spaced base, while the more erectable denticles on the flank have a more narrow base. Elastic fibers help the denticles return to their resting position (A. Lang et al., 2011).

Table 2: Morphological Measurements of flank Denticles (Wen et al., 2014)

Measurement	**Value**	**Unit**
Denticle Length (DL)	151	μm
Denticle Width (DW)	125	μm
Spacing (RS)	51	μm
Denticle Height (DH)	113	μm
Denticle Base Width (BW)	119	μm
Denticle Neck Length (NL)	45.1	μm
Denticle Neck Width (NW)	50.9	μm
Denticle Base Length (BL)	83.8	μm
Height of Midridge (RHM)	21	μm
Height of Side-Ridge (RHS)	11	μm
Height-to-Spacing Ratio (RHM/RS)	0.41	-
Height-to-Spacing Ratio (RHS/RS)	0.21	-

Table 3: Morphological Measurements of flank Denticles (Zhang et al., 2022)

Measurement	**Value**	**Unit**
Denticle Length (DL)	138	μm
Denticle Width (DW)	135	μm
Riblet Spacing (RS)	39	μm
Height of Midridge (RHM)	8	μm
Height-to-Spacing Ratio (RHM/RS)	0.21	-

Dentciles on the flank of the body can reach angles of 50° or more. The erection angle is determined by comparing the visible length of the denticle crown when the denticle is raised to its erection angle versus in the resting position. This angle is measured relative to the skin's surface, when the scale lies flat against the skin, the angle is theoretically 0°. The lateral denticles exhibit larger erection angles (mean angle = $44° \pm 1°$) than the dorsal (mean angle = $26° \pm 1°$) and ventral regions (mean angle = $25° \pm 2°$) (A. Lang et al., 2011). The same was concluded by Motta et al. (2012) and the results of the angles measured on different regions of the body are shown in Figure 5 and listed in Table 4.

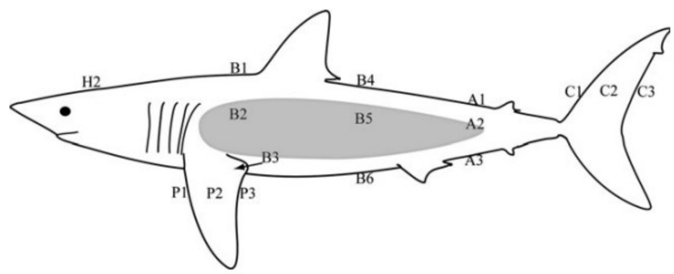

Figure 5: Lateral view of a Shortfin Mako shark illustrating the sampled regions. The flank of the shark is shaded in gray to highlight the area with the highest scale flexibility (Motta et al., 2012).

H2	33°± 1
B1	28°± 1
B2	48°± 1
B3	30°± 1
B4	25°± 1
B5	43°± 2
B6	28°± 1
A1	25°± 1
A2	39°± 1
A3	16°± 3
P1	1°± 1
P2	23°± 1
P3	32°± 2
C1	25°± 2
C2	28°± 1
C3	30°± 2

Table 4: Denticle erection angles (Motta et al., 2012).

2.2 Denticle pattern

The structural composition of the denticles of the shark skin show differences among different parts of the shark's body. Figure 6 shows the denticle patterns and shapes in different areas of the skin from head to tail of two different species of sharks (Small Spotted Cat shark and Starry Smooth Hound shark) (Baeten et al., 2024). This figure clearly shows significant differences between species in denticle pattern and shape, but also differences within one species since the two pictures of the Cat shark were taken in front of and behind the first dorsal fin, respectively.

Wen et al. (2015) conducted an analysis of three different denticle arrangements on biomimetic shark skin and studied the impact of changing the arrangement and spacing on swimming performance. The three arrangements tested are staggered-overlapped, linearly-overlapped and linearly-non-overlapped and are shown in Figure 7.
Wen et al. (2015) tested the different membranes with the dynamic self-propelled swimming tests. The membranes were actuated using a heave motion, which involves lateral, side-to-side movement. Contrary to their expectations, the linear non-overlapping membrane showed the slowest self-propelling swimming speeds. Although the staggered overlapping membrane has a larger total surface area due to the higher number of denticles, the swimming speeds were, on average, nearly 20% higher. The study also found that the staggered overlapping pattern showed the highest self-propelled speeds at all wave conditions tested, outperforming the smooth control and the other shark skin membranes.

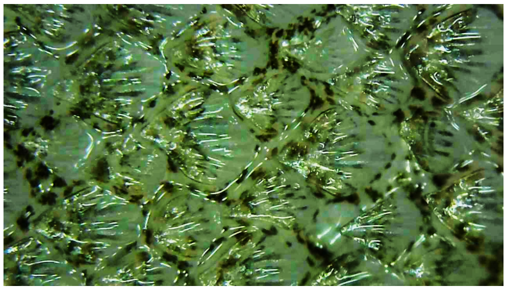

(a) Starry Smooth Hound shark, rounded and widely spaced denticles on top of the head

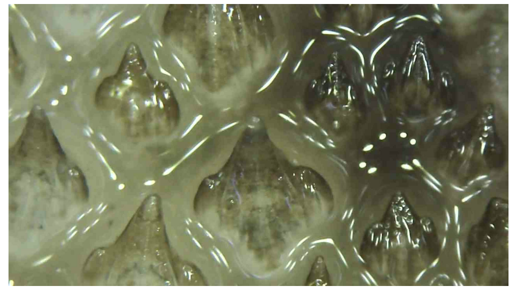

(b) Small Spotted Cat shark, long sharp denticles in front of the dorsal fin

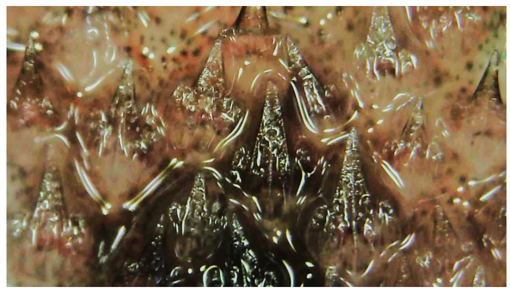

(c) Small Spotted Cat shark, long sharp denticles behind the dorsal fin

Figure 6: Microscopic pictures of structure and arrangement of the denticles of the Starry smoothhound shark and Small Spotted Cat shark (Baeten et al., 2024).

Although the staggered overlapping pattern required more energy to move through the water, as indicated by a higher Cost Of Transport (COT), the significantly higher swimming speeds of this design compensated for the additional effort needed to propel it.

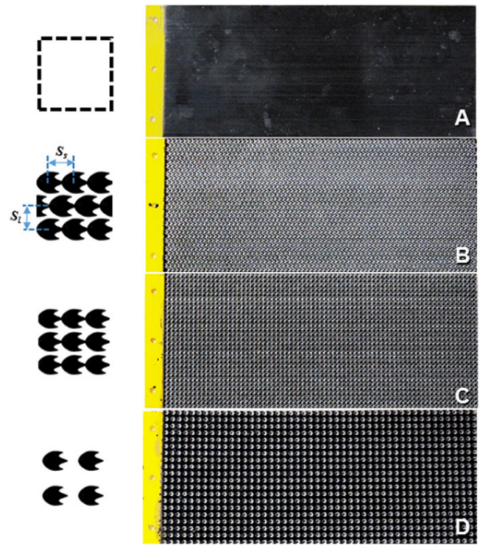

Figure 7: Different denticle arrangement tested by Wen et al. (2015). a) smooth membrane used as the control, b) Staggered-overlapped, c) linearly-overlapped and d) linearly-non-overlapped.

2.3 Hydrodynamics and flow analysis

When a shark swims, it encounters two primary sources of drag: 1) skin friction drag and 2) form drag (A. Lang et al., 2015). Skin friction drag, arising from the friction between the water and the shark's body, is associated with the flow moving over the shark. This type of drag results from the no-slip boundary condition between the water and the shark, forming a boundary layer. High swimming speeds results in a high Reynolds number, leading to turbulent flow across the shark's body and a substantial increase in skin friction. The second type of drag, form drag, is more crucial to control. It originates from pressure differences around the body and depends on whether the flow remains attached or separates during swimming (A. Lang et al., 2015). The water flow experiences a favorable pressure gradient from the nose to the point of maximum girth (near the gills), while unfavorable pressure gradients occur downstream of this point, causing a substantial increase in drag. (A. Lang et al., 2011). This aligns with the observation that for the fast swimming Mako shark the most flexible scales are situated on the body's flanks and downstream of the gills, as shown in Figure 5, regulating flow separation. (A. Lang et al., 2011).
Figure 8a illustrates how denticles contribute to sharks' ability to control form drag. As shown, when the flow encounters an object, vortices form at the point of impact because of a strong unfavorable change in pressure (Du et al., 2022). As they interact with the flow, larger vortices carrying low pressure break away downstream, breaking apart and combining with smaller ones. This causes the flow to separate extensively. However, when the plate is covered in shark-like scales, the situation changes. Vortices that break away from the front edge stay closer to the surface, indicating less separation of the flow compared to a flat plate as shown in Figure 8a.

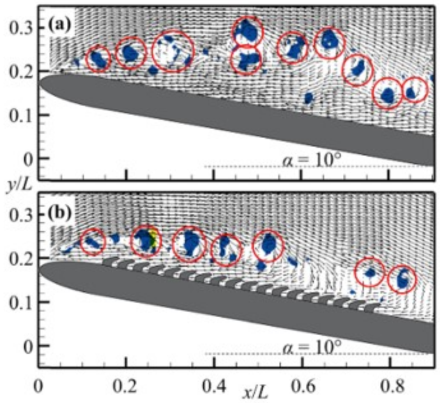

(a) Control of flow separation with biomimetic shark denticles (Du et al., 2022)

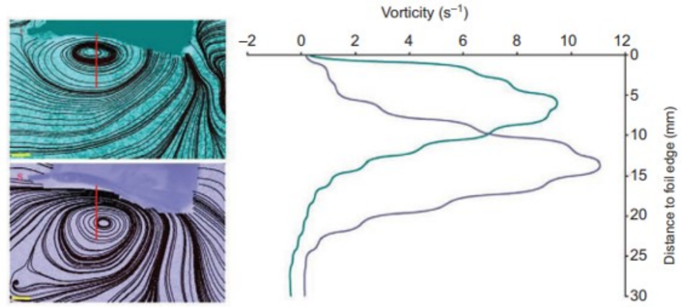

(b) Distance LEV on intact (top) and sanded (bottom) shark skin(Oeffner & Lauder, 2012)

Figure 8: Water flow patterns over shark skin denticles.

Oeffner and Lauder (2012) investigated water flow patterns across shark skin with intact denticles and shark skin whose denticles had been sanded off, using a flapping foil robot that simulates swimming movements. The study observed significant differences in water flow patterns between the two surfaces. Digital Particle Image Velocimetry (DPIV) revealed that the leading-edge vortex (LEV) was positioned further from the foil surface after the denticles were sanded off compared to the intact foil, as shown in Figure 8b. The intact denticles caused the LEV to adhere more closely to the surface, thereby increasing thrust through leading-edge suction. This suggests that shark skin denticles not only reduce drag but also enhance thrust by changing the vortex location. While previous literature has primarily focused on drag reduction, these findings indicate that denticles also increase thrust, particularly on the tail and pectoral fins during maneuvering by improving vortex attachment and lift.

The study of Miyazaki et al. (2018) discusses the morphology of a single denticle of the Galapagos shark and highlights a structure with five ridges and four grooves. This feature, referred to as non-uniform grooves in the study, is defined by distinct differences in height or spacing between the ridges on top of the denticle. The research observes strong longitudinal vortices concentrating at the ridges of shark skin denticles, particularly near the side ridges. Weak longitudinal vortices are noted in the valley of the grooves, suggesting that the multiple-ridge denticles play a role in disrupting longitudinal vortices and weakening secondary flows. This disruption may isolate high shear stress across the grooves, reducing the exposure of a significant portion of the denticle surface to high mean shear. The non-uniform grooves, specifically the unique five-ridge denticles, are highlighted for their morphological significance in passive flow control near shark skin. A systematic Computational Fluid Dynamics (CFD) study explores how the morphology of multi-sharp-ridge denticles, characterized by non-uniform grooves, affects passive turbulent flow control (Miyazaki et al., 2018). The investigation focuses on the hydrodynamic effects of height-to-spacing ratios of mid-ridge and side-ridges. The study found that an increase in non-uniform height-to-height and spacing-to-spacing ratios enhances the strength of longitudinal vortices, clarifying how

non-uniform grooves enhance secondary flows better than uniform grooves.
Overall, the results of the study of Miyazaki et al. (2018) confirm the morphological significance of multiple-ridged non-uniform grooves in passive turbulent flow control near sharkskin denticles.

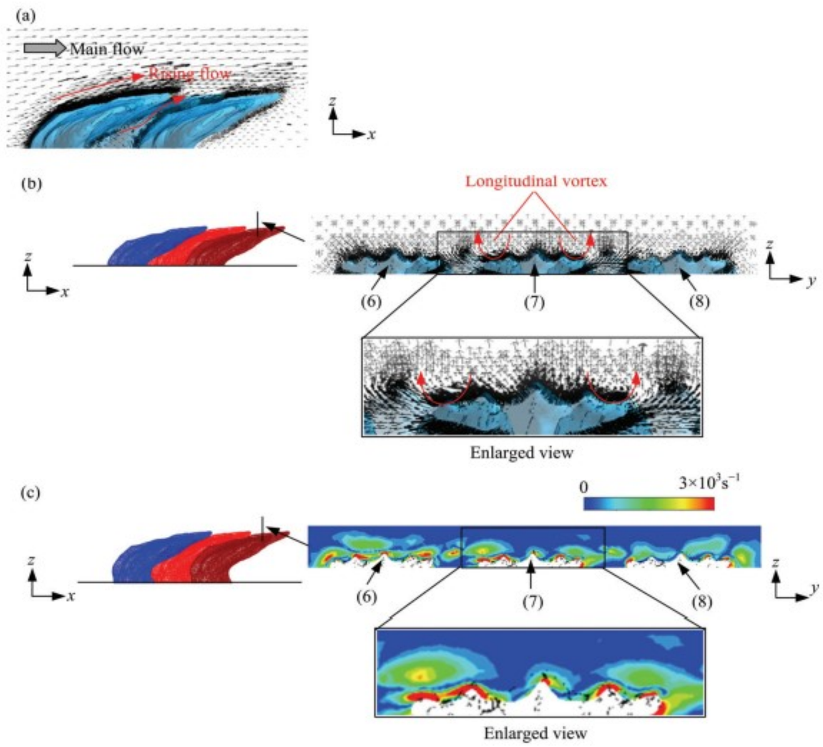

Figure 9: Flow patterns around a denticle model: (a) Velocity vectors in x-z cross-section, (b) velocity vectors in y-z cross-section, and (c) iso-vorticity ($|\omega_x|$) contours in y-z cross-sections (Miyazaki et al., 2018)

As mentioned before, the Shortfin Mako shark has loosely anchored denticles across its body that, through a flow-activated mechanism, can control the separation of the flow, thereby reducing resistance (Patricia et al., 2019). The study of Afroz et al. (2017) tested the skin of Shortfin Mako sharks, specifically from the flank region with highly movable scales, under various adverse pressure gradients (APG) to assess its ability to control separation in fluid flow. The results showed that shark skin can effectively control both laminar and turbulent separation on a flat, non-moving surface. Furthermore, the presence of shark skin on the flat plate resulted in a smaller separation region and a delayed separation point under different magnitudes of APG.

Wen et al. (2015) conducted research on the swimming performance of biomimetic shark skins and suggested that the flexibility or bristling of denticles in real shark skin may also play a role in reducing the energetic costs associated with denticle interactions during heaving locomotion. Sharks with loosely embedded denticles in the epidermis and dermis could achieve hydrodynamic benefits without incurring higher COT due to denticle interactions and friction while arching its body.

3 Methods and Materials

This chapter provides a comprehensive overview of the development of biomimetic shark skin design. It explores the conceptualisation process, material selection and the applied assembly method.

3.1 Design and prototyping

3.1.1 Biomimetic replication

Different techniques for manufacturing biomimetic shark skin are discussed by Pu et al. (2016). Three primary approaches are examined: 1) the bio-replicated forming method, 2) direct fabrication of surface microstructures and 3) indirect fabrication of surface microstructures.

The bio-replicated forming method consists of replicating surface microstructures using real biological surfaces as templates as shown schematically in Figure 10a. The negative mold is made by pouring a polymer over real shark skin. Subsequently, a polymer is poured over the negative mold to create a realistic shark skin replica (Han & Zhang, 2008; Pu et al., 2016). Although this method is effective for high fidelity to biological templates, it is constrained by limited resources and cost, making it unsuitable for large-scale applications.

The direct fabrication method constructs microstructures without a negative template and instead uses techniques such as surface machining to create the biomimetic samples as shown in Figure 10b. Although this method offers competent designs, it is generally limited to small area applications due to cost and efficiency limitations.

The indirect manufacturing method also makes use of a negative mold which captures a shape or form of the object in a reversed or negative way as shown in 10c. In contrast to the bio-replicated forming method, this technique involves the direct fabrication of the negative mold itself, instead of casting a polymer over an existing biological template.

Given the need for integrating the actuation mechanism within both the membrane and denticles, opting for the indirect manufacturing method appears to be the most suitable approach.

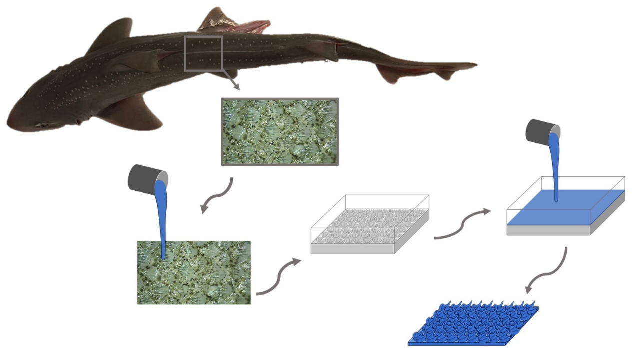

(a) Bio-replicated forming

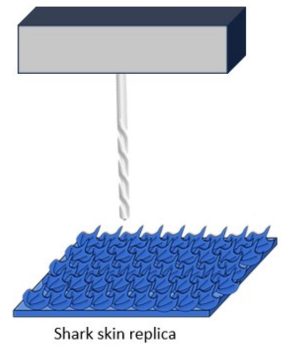

(b) Direct fabrication method

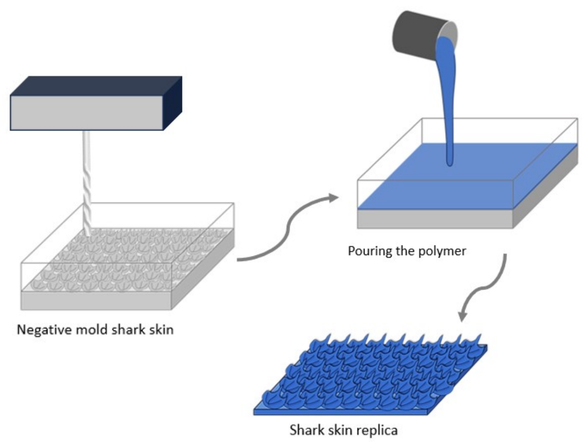

(c) Indirect fabrication method

Figure 10: Basic principle of techniques for manufacturing biomimetic shark skin (Baeten et al., 2024)

3.1.2 Denticle design

The morphology of the denticles discussed in the previous chapter was applied to a denticle design. The design of the shape of the denticle includes a combination of denticles in three different locations, with each location having a crucial function in optimizing the hydrodynamic advantage along the body of the Shortfin Mako shark. The dimensions of the 3D constructed denticle are selected either as the average of the measurements taken from Table 1, 2 and 3, or as values within the range of those measurements. The design features three ridges and a narrow base, a characteristic commonly found in the denticle structure of the Shortfin Mako shark, as illustrated in Figure 4a and b. The dimensions applied are listed in Table 5. This design served as the blueprint for creating multiple 3D printed molds to replicate the intricate features of the denticles. The definitive denticle design was completed in SolidWorks and is shown in Figure 11.

While the proportions of the denticles remained as true as possible to those found in nature,

Table 5: Morphological dimension 3D constructed denticle

Measurement	**Value**	**Unit**
Denticle Length (DL)	163	μm
Denticle Width (DW)	140	μm
Riblet Spacing (RS)	44	μm
Denticle Height (DH)	110	μm
Denticle Base Width (BW)	81	μm
Denticle Neck Length (NL)	44	μm
Denticle Neck Width (NW)	30	μm
Denticle Base Length (BL)	40	μm
Height of Midridge (RHM)	60	μm
Height of Side-Ridge (RHS)	40	μm

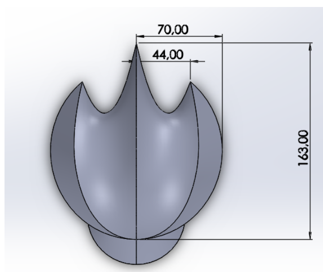

(a) Top view

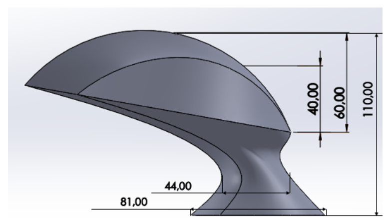

(b) Side view

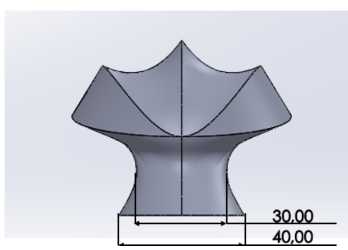

(c) Front view

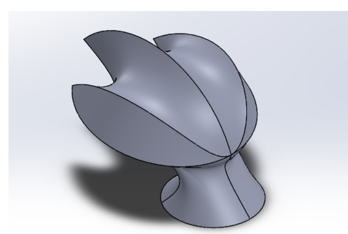

(d) Iso view

Figure 11: Top, side, front and isometric view of a 3D reconstructed SolidWorks model of a denticle. Dimensions are in μm.

adjustments were made to accommodate the limitations of the printing process, as well as design challenges that were encountered. Despite this deviation, the fundamental proportions and characteristics of the denticle design were maintained to preserve the biomimetic integrity of the replica as best as possible. One modification that deviated most significantly from the denticle's original proportions was increasing the thickness of the denticle ridges. While the Mako shark has very thin ridges along its body flanks as shown in Figure 4, this design incorporates thicker denticle ridges. This modification enhances the actuation mechanism, making it easier and more efficient to assemble. This will be discussed in further detail in a subsequent chapter.

3.1.3 Denticle bristling mechanism

To gain a comprehensive understanding of the bristling effect, it is essential to examine its mechanism in the Shortfin Mako shark, as illustrated in Figure 12. A. W. Lang et al. (2014) showed that the scales are able to erect only by the reversal of the water current, without requiring body movement or an active muscular contraction mechanism, as previously believed. As a result, the skin surface of the shark serves as a passive, flow-actuated dynamic micro-roughness. This was also later proven by Du Clos et al. (2018), who analyzed video footage of water flow over the skin of a shortfin Mako shark, as shown in Figure 13.

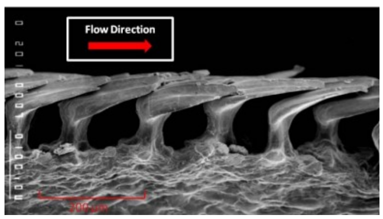

(a) SEM image of non-bristled denticles

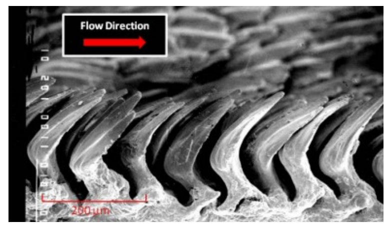

(b) SEM image of manually bristled denticles

Figure 12: Bristling of dermal denticles from the flank (Afroz et al., 2017).

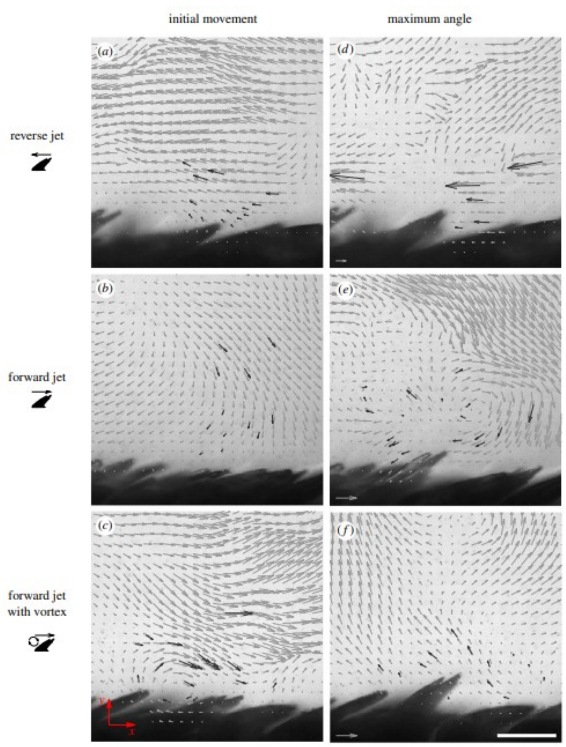

Figure 13: Velocity fields of three different water flows over shark denticles (Du Clos et al., 2018).

This highlights the mechanism of a single denticle. However, the orientation of denticles is also influenced by the swimming motion of the shark. Figure 14 illustrates the complete mechanism of bristling in a swimming shark. During locomotion, water flow tends to separate from the shark's body, which, as previously discussed, increases drag force. The denticles mitigate this separation, ensuring that the flow remains attached to the body surface, thereby reducing drag. Additionally, the bristling effect of the denticles further enhances this drag-reducing property.

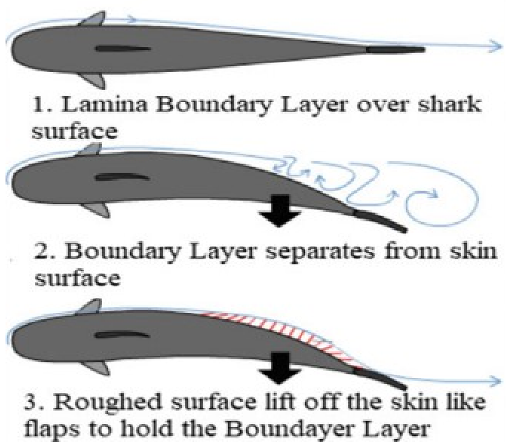

Figure 14: Bristling effect of the denticles during swimming (Livya et al., 2019).

To replicate this mechanism, the bristling effect in sharks can be categorized into two distinct activation mechanisms. Each mechanism contributes to the dynamic adaptation of the denticles.
Firstly, the loosely anchored nature of each denticle within the skin affords them a degree of freedom, allowing for subtle movement, as shown in Figure 12 and 13. This inherent flexibility enables the denticles to adjust position in response to hydrodynamic forces encountered during swimming.
Another contributing factor to the bristling effect is the swimming motion of the shark. The shape of the shark's body during swimming affects the spacing between its denticles. On the concave side, where the body curves inward, the denticles naturally come closer together. Conversely, on the convex side, where the body curves outward, the denticles tend to spread apart, as shown in Figure 15.

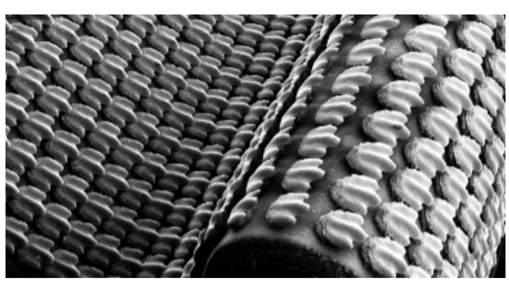

Figure 15: Spacing between denticles convex and concave side (Lauder, 2015).

3.1.4 Actuation of denticle bristling mechanism

As previously mentioned, the bristling effect of the Mako Shark is a passive, flow-actuated mechanism. However, in the design of this biomimetic shark skin, an active actuation mechanism will be implemented. Due to the application of the indirect fabrication method, the shark skin will be composed of a flexible material. Consequently, various actuation options commonly employed in soft robotics were considered. As a rapidly evolving field, soft robotics provides innovative techniques for imparting motion to flexible polymers. For instance, by strategically integrating materials into the membrane, an external trigger can prompt them to undergo a transformation, causing the membrane to adopt a convex shape or the denticle to erect a certain angle.

Wang and Chortos (2022) discussed different actuation strategies in this domain, such as fluidic-driven, electric-driven, and magnetic-driven actuators.

Fluidic actuation, which includes pneumatic and hydraulic systems, uses pressurized gas or liquid to deform soft materials, providing strong forces and flexibility, especially for underwater applications.

Electric actuation involves converting electrical energy into mechanical deformation either directly, as in dielectric elastomers or piezoelectric materials, or indirectly through heat or light, enabling precise and high-speed control.

Magnetic actuation uses magnetic fields to generate movement or alter material properties, either directly by interacting with ferromagnetic or paramagnetic materials or indirectly by converting magnetic energy into heat or other forms (Wang & Chortos, 2022).

Table 6 presents the dvantages and disadvantages of various actuation mechanisms potentially applicable to shark skin design. Certain options, such as hydraulic actuation under fluidic actuators, have been omitted as this would be an overly robust solution for the small actuation that would be needed here.

Given the inherent complexity of designing shark skin with denticles, the simplicity of the actuation mechanism became a critical requirement. The chosen mechanism needed to be not only easy to actuate but also straightforward to integrate into the overall shark skin structure. Pneumatic actuation would significantly complicate the skin design, as it would require the incorporation of air pockets, adding layers of complexity to the overall structure. Additionally, both magnetic and direct electric actuators presented substantial challenges, with their primary drawbacks being limited strength and insufficient deformation capabilities. These limitations made them less suitable for achieving the dynamic and flexible movements required for the shark skin design. Among the various options considered, one actuator quickly emerged as the most suitable: shape memory alloys (SMAs), particularly Nitinol. This material stood out due to its unique ability to provide the necessary actuation while maintaining the simplicity required for seamless incorporation into the intricate shark skin design.

Table 6: Advantages and disadvantages of soft robotic actuation mechanisms; *Pneumatic actuator (Gariya et al., 2023), Dielectric elastomer (Kim et al., 2013), Shape memory alloy (Chafik et al., 2022), Magnetic silicone elastomer(Khoo & Liu, 2001)*

<table>
<tr><th></th><th>Actuation mechanism</th><th>Pros</th><th>Cons</th></tr>
<tr>
<td>Fluidic Actuator</td>
<td>Pneumatic systems
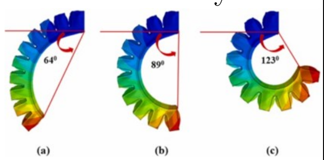</td>
<td>High force output
The actuation force and speed can be easily adjusted by varying the fluid pressure.</td>
<td>Requires complex control systems to manage fluid flow, pressure, and actuation sequences.
Pneumatic systems require regular maintenance to avoid leaks, ensure proper air quality, and maintain system integrity.</td>
</tr>
<tr>
<td>Electric Actuator</td>
<td>Direct: Dielectric elastomers, piezoelectric materials.
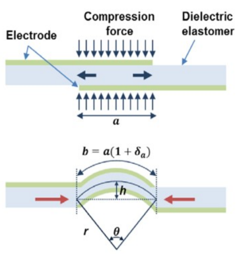
Indirect: Shape memory alloy (SMA)
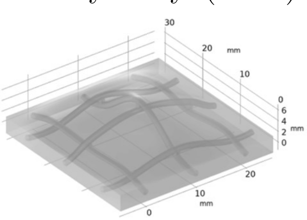</td>
<td>Direct:
Precise control over motion, positioning, and force.
Can be compactly designed for small or intricate systems.
Indirect:
Generate significant force relative to their compact size.
Actuation is simple, using heat-triggered shape changes.</td>
<td>Direct:
Actuators are characterized by their ability to produce small, precise motions.
Produce small output forces
Indirect:
SMAs can suffer from fatigue over time, leading to reduced performance or failure.</td>
</tr>
<tr>
<td>Magnetic Actuator</td>
<td>Ferromagnetic or paramagnetic materials
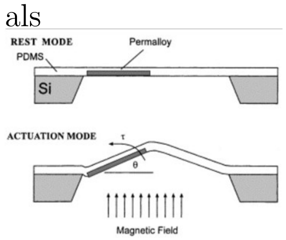</td>
<td>Minimal moving parts, reducing chances of wear and maintenance needs.
Offers precise control over the bristling effect.</td>
<td>Magnetic actuators typically generate less force.
Requires exact control of magnetic fields, which can be technically challenging and require complex setups.
The effectiveness of magnetic actuation diminishes with distance from the magnetic source, limiting the range of operation.</td>
</tr>
</table>

3.1.5 Bristling mechanism design parameters

The material of which the entire shark skin will be made is a silicone-based material selected for its flexibility and workability. Both the membrane and denticles are made of Ecoflex 00-10 silicone so that the Nitinol wires can actuate the denticles locally as well as the membrane globally.
For this reason a mold was 3D printed made of Durable Resin V2 using a Formlabs 3B printer, the optimal mold design is presented in Figure 16. First, a design was created in SolidWorks with 6 dentciles lined up in a row. The design of the denticles correspond to the specifications detailed in the chapter on denticle design. Subsequently a negative mold is created from the row of denticles as shown in Figure 16b.

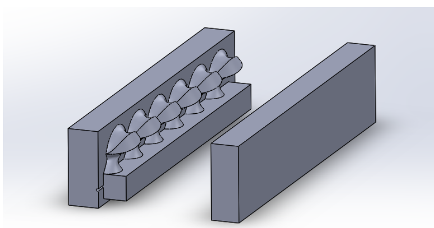

(a) 3D model of mold casting of a single row of denticles

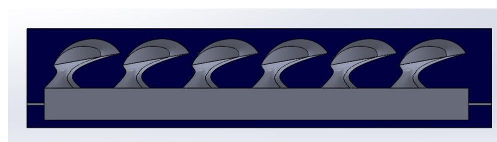

(b) Left side of the 3D printed mold

Figure 16: Casting mold.

Three different diameter Nitinol wires were tested; 0.3, 0.5 and 1 mm diameter wires. It was found that for membrane activation, the 0.3 mm and the 0.5 mm diameter wires are not strong enough to actuate the movement. For actuating the local bristling mechanism of a single denticle, all 3 diameter wires are suitable, however since the wire has to be a completely closed circuit it will form a loop in the crown of the denticle where space is limited. For this reason, it was most plausible to choose 0.3 mm diameter.
In Figure 17a, Wen et al. (2015) demonstrates the swimming motion with a biomimetic shark skin and Figure 17b presents a side view. This clearly shows that the space between the denticles becomes larger at the peak compared to the denticles in the valley. In Figure 18, the design parameters of the swimming motion and the loosly-anchored denticle, which together produce the overall bristling effect, are illustrated. This design allows for multiple combinations. As previously discussed, the angles that the denticles can form relative to the skin vary significantly around the body of the Mako shark. Additionally, due to the swimming motion of the shark, the curvature varies of different parts of its body. The body bends more at the tail than at the head. Consequently, this results in a range of combinations, leading to varying angles and distances between the denticles. The design of the actuation mechanism allows for both the local and global mechanisms to be adjusted and controlled separately.

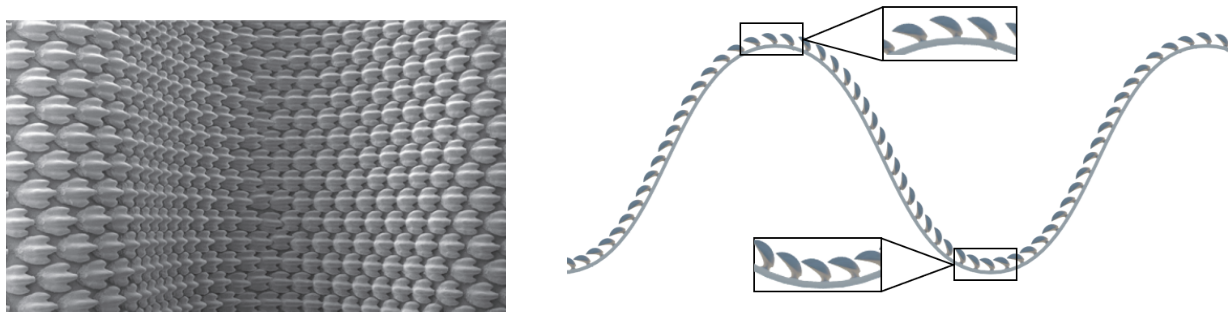

(a) Replication of swimming motion of staggered-overlapped biomimetic shark skin membrane (Wen et al., 2015).

(b) The side view of swimming motion of staggered-overlapped biomimetic shark skin membrane

Figure 17

The global mechanism involves actuating an entire row to create a curve. The extent and direction of this curve can be predetermined changing the parameters shown in Figure 18, allowing the mold to be customized accordingly.
This approach also applies to the local mechanism of the individual denticle. The angle (α) at which the denticle aligns with the skin can be adjusted through the programming of the local actuation mechanism. By making adjustments to the design of the casting mold used to shape the denticles with silicone, the density of the entire grid of denticles can also be altered. This allows for the modification of many parameters to achieve the desired final design. The parameters chosen for this design are described below.

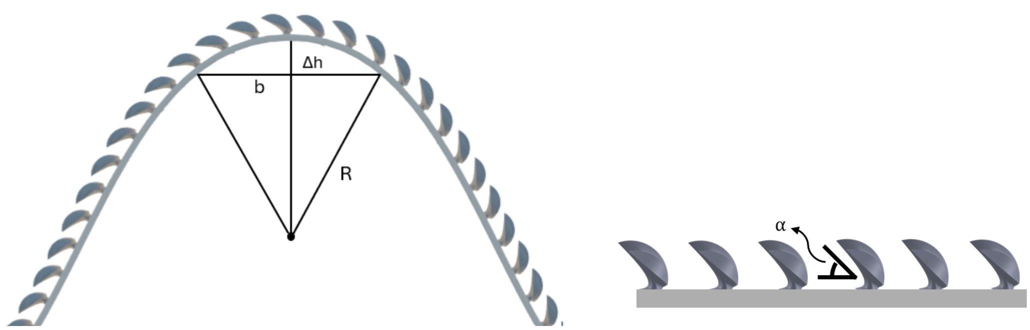

(a) (b)

Figure 18: Design parameters bristling mechanism biomimetic shark skin. R = Radius of the circular arc or curvature, b = Chord length of the circular arc, Δh = Vertical deviation relative to a flat membrane, α = angle between denticle top and skin.

3.1.5.1 Global bristling mechanism and body curvature

To gain a deeper understanding of the mechanism behind a shark's swimming motion, it is essential to look at how much the body flexes and what effects this flexing has. The head and anterior portion of the body experience minimal lateral displacement, while the mid-body demonstrates moderate lateral flexion.
Oeffner and Lauder (2012) conducted research on biomimetic shark skins inspired by the Shortfin Mako shark, testing them with a device simulating swimming motions. This was aimed at achieving a curvature similar to that of the spiny dogfish mentioned in the study, which exhibits a curvature ranging between $\kappa = 0.14$ and 0.20 cm^{-1}. By achieving comparable curvature values, the biomimetic skin may exhibit the same range of curvature to live sharks. The formulas and calculations used to determine the radius of swimming motion are shown below. Δh and the radius are shown in table 7.
Curvature:

$$\kappa = \frac{1}{R}$$

$$(R - \Delta h)^2 = R^2 - \left(\frac{b}{2}\right)^2$$

$$R - \Delta h = \sqrt{R^2 - \left(\frac{b}{2}\right)^2}$$

$$\Delta h = R - \sqrt{R^2 - \left(\frac{b}{2}\right)^2}$$

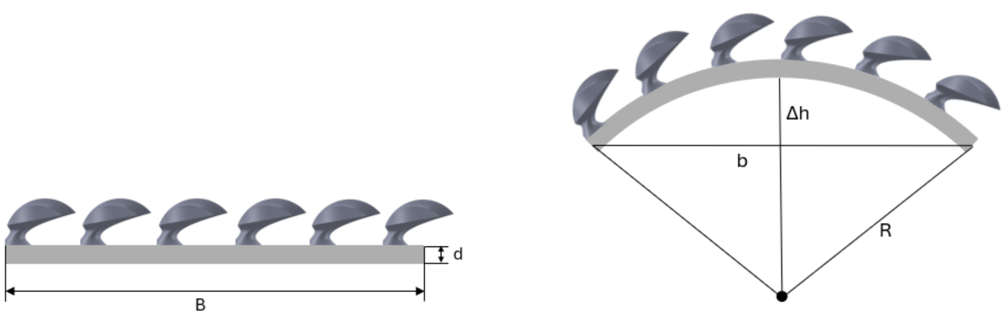

(a) Flat membrane (b) Actuated membrane

Figure 19: Bending of the membrane. R = Radius of the circular arc or curvature, B = Length of denticle row, d = Thickness, b = Chord length of the circular arc, Δh = Vertical deviation relative to a flat membrane.

The row of biomimetic denticles, shown in Figure 19, will have a length of B = 13 cm and a thickness of d = 1 cm. The Δh calculations were obtained with a b of 10, 11 or 12 cm. As the denticle row bends, the ends come closer together and a distance between 10 and 12 cm will be expected. A mold is created to hold the Niti wires, allowing them to be heated into

Table 7: Δh values if b = 10 cm, 11 cm or 12 cm

Curvature (cm^{-1})	Radius (cm)	Δh (cm)	Δh (cm)	Δh (cm)
0.14	7.14	2.04	2.58	3.26
0.17	5.88	2.79	3.8	-
0.19	5.26	3.63	-	-
0.20	5	-	-	-

the desired shape. A subsequent chapter will explain the functioning of Nitinol in detail. A Δh of 3.63 cm was chosen from Table 7 when designing the mold for the NiTi wire. and is shown in Figure 20.

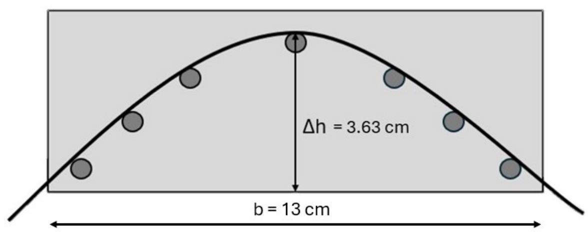

Figure 20: Dimensions of the mold holding the Niti wire for the global bristling mechanism.

3.1.5.2 Local bristling mechanism

The bristling of the loosely anchored denticle represents a localized form of the mechanism. This mechanism by which a denticle executes a bristling movement can be characterized as a hinge-like action.

Due to specific considerations in the global bristling mechanism and the three commonly used options for designing the denticle structure, a silicone base was selected. This material can embed an actuation mechanism and is both flexible and elastic, effectively capable of mimicking natural movement of shark denticles. Since the entire structure will be made of silicone, it will have sufficient flexibility to allow for local bristling and flexion. The denticle design incorporates a narrow base, which serves as the pivot point for the bristling effect, functioning as a hinge.

The angle at which the denticles orient themselves is derived from the research of Santos et al. (2021), which demonstrated that denticles inclined up to 50 degrees are more effective at preventing flow separation compared to those at 30 degrees. Furthermore, 50 degrees is, on average, the maximum angle that denticles on the shark's flanks can achieve. As a result, a mold was created to adopt this angle for the activation mechanism, which is illustrated in Figure 21. The wire shown in the figure is part of the activation mechanism and will be elaborated upon in a subsequent chapter.

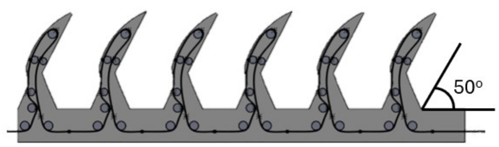

Figure 21: Angle of the localized brisling mechanism

3.2 Shape Memory Alloy: Nitinol

3.2.1 NiTi wire

The thermal-induced Shape Memory Effect (SME) is illustrated in Figure 22 (Kumar Patel et al., 2020). The material undergoes a cyclic journey from points A to B to C to D and eventually returns to point A. This cycle enables the material to recover its original shape by transitioning from a deformed state (martensite) to its initial state (austenite). To activate this shape memory effect, the material must be maintained at a temperature below a specific threshold known as the Martensitic finish (Mf) temperature (Kumar Patel et al., 2020).
As the material undergoes loading (along curve A-B), it deforms while staying within its stress limit. When the load is removed (from point B), there is a minor release of strain (point C). Initially, the material assumes a particular configuration known as twinned martensite, which is pivotal for enabling the shape memory effect. Loading triggers a change in this configuration, shifting it to detwinned martensite, a transformation process called martensite transformation.
Recovery of the original shape (curve C-D) occurs when the material is heated. This recovery begins at a certain temperature known as the Austenitic start temperature (As) and ends at the Austenitic end temperature (Af). However, despite this recovery, the crystal structure of the material remains slightly altered from its initial state, requiring a subsequent cooling process to return the material to its original shape. The optimal shape-setting temperature (Af) for Nitinol typically falls within the range of 500–550°(Bengisu & Ferrara, 2018).
During the cooling phase, only twinning occurs within the material. This alteration in the crystal structure, particularly in detwinned martensite, induces strain, resulting in deformation. This comprehensive explanation sheds light on the intricate mechanisms underlying the thermal-induced SME, clarifying the interplay between temperature, stress, and material structure (Kumar Patel et al., 2020).

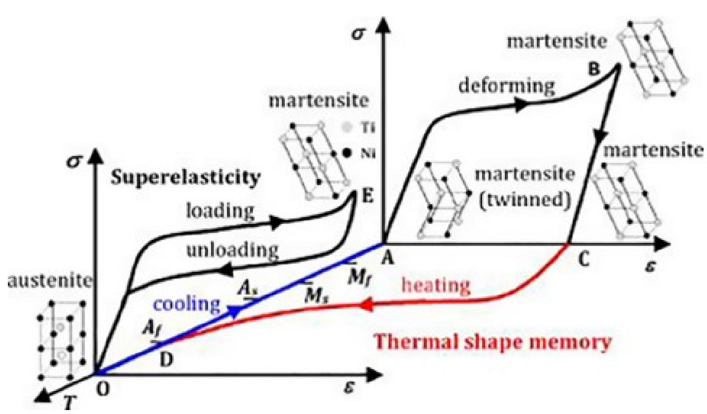

Figure 22: Cyclic journey Thermal-induced Shape Memory Effect (SME)

3.2.2 Temperature development in the Nitinol wire

To achieve the desired Austenitic start temperature, electricity can be applied to heat the wire. Functioning like a conventional wire within an electrical circuit, it warms up due to the Joule effect (Koiri & Sharma, 2021). The electrical power (P) required for this heating can be calculated using the following formula:

$$P = I^2 * R = (\frac{I^2 * \rho * l}{S})$$

Where I = current, R = resistance, ρ = resistivity of Nitinol, l = length of wire, S = cross section of wire.
Here, power represents the heat generated within the wire per second. While a portion of this heat is utilized for work, the majority dissipates into the surrounding environment. This dissipation process is governed by the equation:
Heat of wire = Heat development - Heat lost

$$H_{wire} = I^2 * Rt - h * A(Tw - Ts)$$

where I = current, R = resistance, t = time, h = convective heat transfer coefficient of surrounding, A = surface area of wire, Tw = Temperature of wire, Ts = Temperature of surrounding.
Koiri and Sharma (2021) conducted experiments with Nitinol wires of different diameters within an electrical circuit. The objective was to observe the temperature development in the wire with respect to the current passing through it. The resulting data are displayed in the following graph. At low current levels, the temperature of the 1 mm thick wire remains below 30 degrees, whereas the 0.3 mm thick wire reaches the activation temperature with ease.

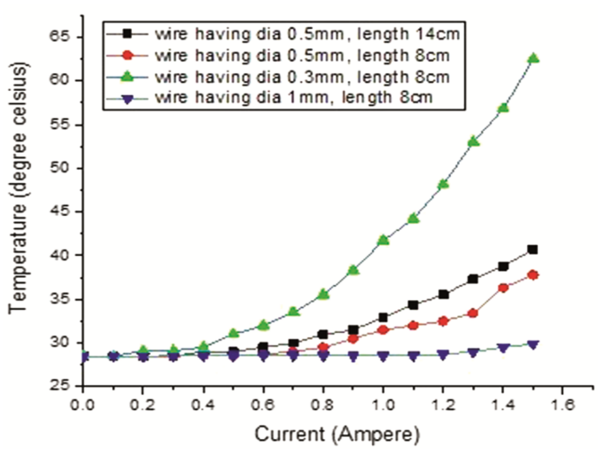

Figure 23: Temperature variation with current across different wires.

An independent experiment was carried out to measure the time until the Nitinol wire reaches 40 degrees, which is the activation temperature of the wire selected in this design. The wires in this study were all 20 cm long and the temperature is measured in the middle, shown in Figure 24. The results are in Figure 25. A high measurement of time is seen at low current levels, which is due to the temperature failing to exceed the 40-degree limit, resulting in the test being stopped after 240 seconds. This is similar to the results in Figure 23. Figure 25b shows the time it took to reach 40 degrees while the wire was embedded in silicone. The wire was encased in silicone with dimensions of 1 cm by 1 cm by 10 cm. A noticeable increase in activation time necessary to bring the wire up to the 40 degree temperature was observed, particularly with the 1 mm and 0.5 mm diameter wires.

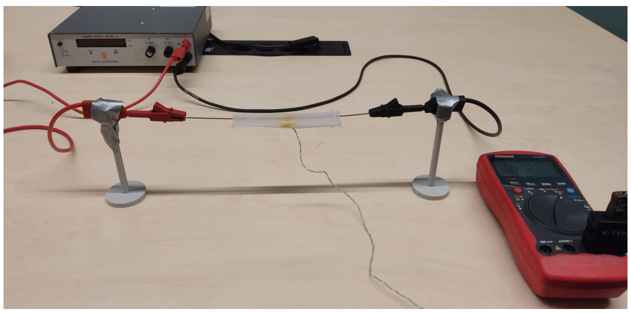

Figure 24: Test setup for testing temperature response of Nitinol wire.

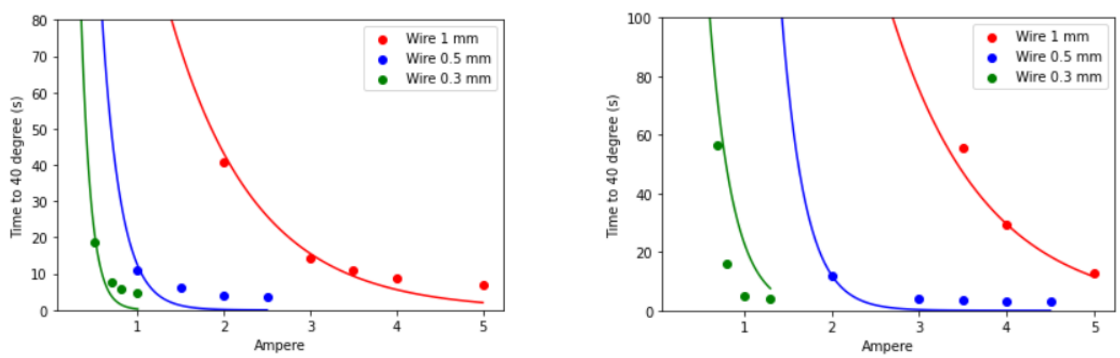

(a) Raw wire

(b) Encased in silicone

Figure 25: Temperature response of Nitinol wires under varying current levels

3.2.3 Characterization of the actuation mechanism

Further characterization of the motion of the two mechanisms is provided here. Figure 26 illustrates the local bristling mechanism. On the left, the figure shows the appearance of the row of denticles when not actuated, while the right side shows the appearance after a current flows through the Nitinol wire. The denticles form an angle of approximately 50 degrees with the base, matching the design specifications of the wire mold.

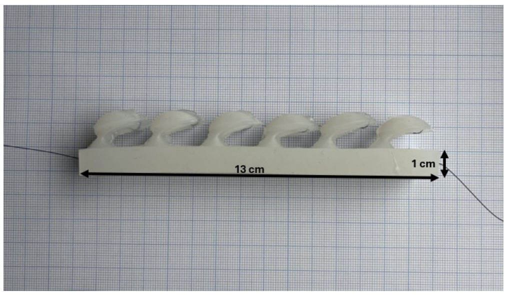

(a) Initial position

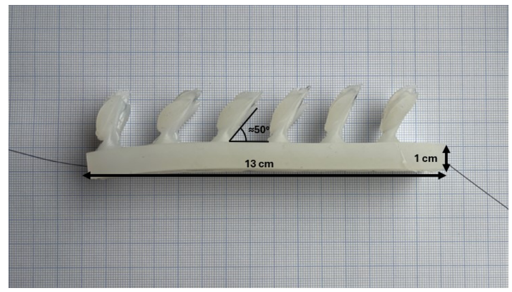

(b) Actuated position

Figure 26: Local actuation of a single row of denticles

Figure 27 demonstrates the actuation of the global mechanism, with the right side displaying the actuated state. Dimensions have been added for clarity. For example, the displacement in the middle is approximately 3 cm, the distance between the two ends of the row is 11 cm, and the length of the curve remains 13 cm. The following formulas, also described in an earlier chapter, were used to calculate the curvature of the row of denticles.

$$\Delta h = R - \sqrt{R^2 - \left(\frac{b}{2}\right)^2}$$

$$3 = R - \sqrt{R^2 - \left(\frac{11}{2}\right)^2}$$

$$(R-3)^2 = R^2 - 30.25$$

$$R = 6.54$$

$$k = \frac{1}{R} = \frac{1}{6.54} = 0.153cm^{-1}$$

The curvature is 0.153 cm, which aligns with the curvature values observed in the Spiny dogfish.

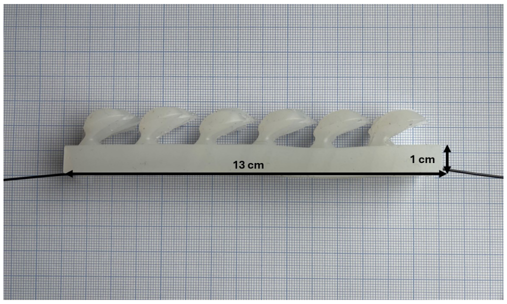

(a) Initial position

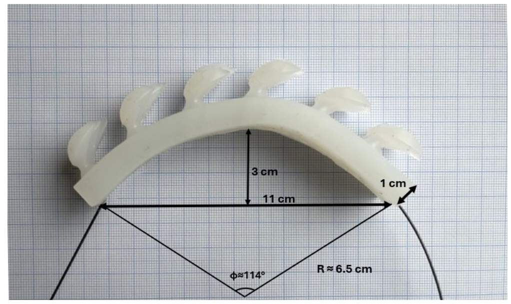

(b) Actuated position

Figure 27: Global actuation of a single row of denticles

3.3 Fabrication process

The fabrication of a biomimetic shark skin replica involved a multi-step process integrating various materials and techniques. To create a grid of denticles, molds were constructed row by row, as shown in Figure 28. Initially, the NiTi wires are strained within a mold and programmed to adopt a specific shape upon electrification. This figure displays two different molds: the upper mold is designed for a 0.3 mm wire, intended to provide local denticle actuation, while the lower mold is designed for a 1 mm wire to provide membrane actuation. A height of $\Delta h = 3.63cm$ was applied for the 1 mm wire, as listed in Table 7. Subsequently, a gas burner was used to heat the wire to its optimal shape-setting temperature, which exceeds 500°C.

Each row's left and right halves were individually crafted by pouring silicone into the mold with the 0.3 mm wire in place, positioned before the silicone was poured in the mold. The left mold was not taken exactly in the centre but a little to the right. Therefor, when the wire is positioned in the left-side mold and silicone is poured over it, the wire will be in the middle when the two halves are bonded together. In this mold, a small groove has been made for this purpose on one side to allow the wire to eventually stick out. This is represented in the fourth step of the fabrication process depicted in Figure 28. To remove air bubbles from the silicone, it was placed in a vacuum chamber beforehand. The two halves of each denticle row were bonded together using Elastosil E43, with the 0.3 mm NiTi wire already in place. The 1 mm wire was positioned between the two halves before bonding, thus completing the integration of the actuation mechanism into a single denticle row.

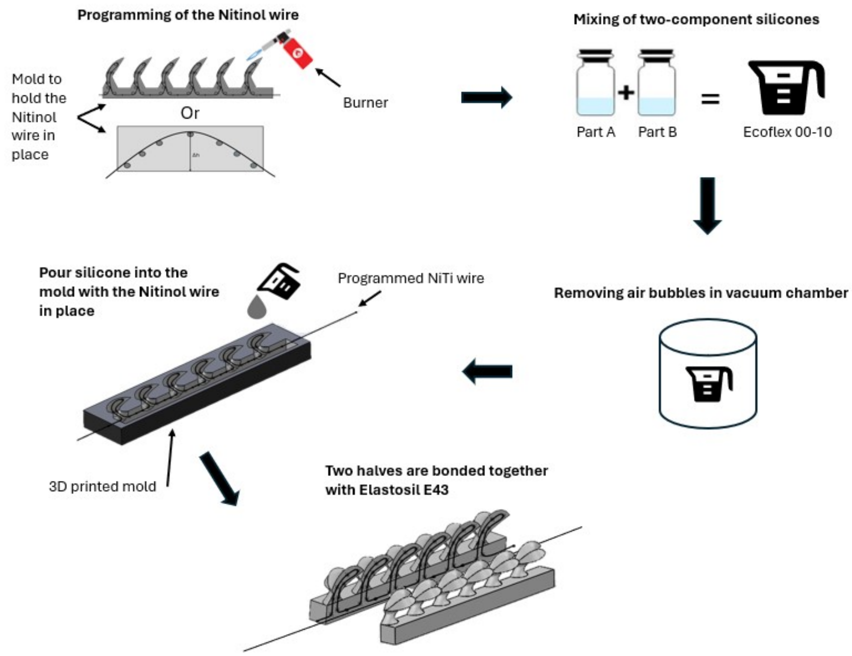

Figure 28: Fabrication process for one row of the biomimetic shark skin.

4 Test setup Analysis

In this chapter, the experimental setup using Particle Image Velocimetry (PIV) measurements performed in a water tank is described.

4.1 Test set-up

To test whether the bristling mechanism still works underwater and whether it has a desired effect, the sharkskin was placed in a water tank and tested with Particle Image Velocitry (PIV). The water tank has the dimensions 100x40x39.5 cm and is shown in Figure 29. PIV is an optical method used to measure the velocity field of a fluid flow. It involves capturing the movement of seeded particles in the fluid to infer the velocity distribution within the flow. PIV measurements require the following components and the specific components used in this test setup are discussed below.

Pump
To generate a flow within the water tank, a pump was utilized. Aqua Medic EcoDrift 4.3 aquarium pump with diffuser of a diameter of 6cm is used. The flow rate was set to 4000 Lh^{-1}.

Illumination
A laser or other light source is used to create a thin sheet of light, which illuminates a specific plane in the fluid where measurements are to be taken. The particles scatter the laser light, making them visible. In this test set-up the flow is illuminated using the LaVision pulsing

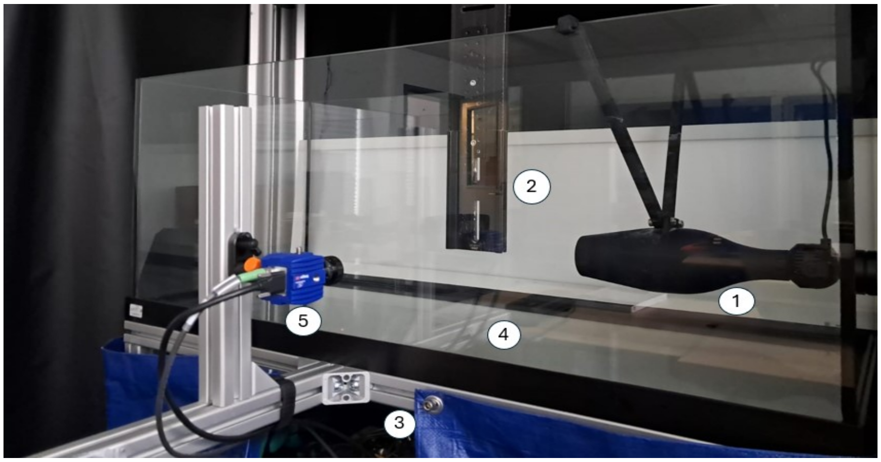

Figure 29: Experimental setup using Particle Image Velocimetry with components: Aqua Medic EcoDrift 4.3 aquarium pump with diffuser (1), Biomimetic sharkskin mount (2), LaVision pulsing LED line light (3), Slit for light passage (4), Imager MX 2M-160 CMOS camera (5)

LED line light.

Image Acquisition
A high-speed camera take consecutive images of the illuminated particles in quick succession, with a known time interval between the images. These images capture the positions of the particles at different moments in time. The camera used for this measurement was the Imager MX 2M-160 CMOS camera. The cameras, equipped with a lens of 16 mm, with a resolution of 1936 pixels × 1216 pixels and pixel size: 3.45 µm × 3.45 µm.

Seeding the Flow
The fluid is seeded with small, neutrally buoyant particles that are small enough to follow the flow accurately without affecting it. The particles are Polyamide HQ with a diameter of 60 µm and a density of 1.03 g/cm^3. These particles serve as tracers that move with the fluid.

Cross-Correlation Analysis
Davis 10.2.1 was used for flow calculations. The images are divided into smaller regions called interrogation windows. These are small sections of the image where particle movement will be analyzed. The vector calculation involves a two-step process with different interrogation window sizes:
First Pass: A larger interrogation window of 64x64 pixels is used to obtain an initial estimate of the particle displacements. This larger window helps to identify the general flow features and provides a preliminary velocity field.
Second Passes: Three subsequent passes use smaller interrogation windows of 48x48 pixels to refine the velocity measurements. The smaller windows provide higher spatial resolution and more detailed information on particle movement, improving the accuracy of the velocity field.

A cross-correlation function is used to compare the particle patterns between the two images within each interrogation window. This process identifies the most likely displacement of particles within that window, yielding a displacement vector.

Velocity Field Calculation
The time between the two images is known, so the displacement vectors can be divided by this time interval to calculate the velocity vectors. By performing this analysis across all interrogation windows, a comprehensive map of velocity vectors is generated, representing the flow field in the plane of interest.

Post-Processing
The calculated velocity vectors are validated to remove erroneous data points, often caused by noise or inadequate seeding.

4.2 Different Test Configurations

The biomimetic shark skin will be tested with two different configurations of denticles: linearly-overlapped and staggered-overlapped membranes. Additionally, a third configuration will involve testing a single denticle placed in the water tank. These configurations are depicted in Figure 30. The three different configurations are tested twice: first, when they are not actuated and at rest, and second, when they are actuated to demonstrate the bristling effect. The difference between the two settings is shown in Figure 31.
The two membranes are positioned so that the camera is focused on the tops of the denticles. In this setup, the light shines from below, evenly illuminating the surface just in front of the denticles. For the single denticle, the orientation differs; it is placed in front of the pump, with the camera focused on its side. Here, the light shines upward through the center, creating a 2D plane that slices through the middle of the denticle. Sharkskin membranes were positioned 2 cm in front of the pump nozzle. The single denticle was mounted on clear plexiglass, placed 14 cm from the pump nozzle to ensure adequate water flow development over the plexiglass surface.
Before testing the various denticle configurations in the water tank, it was essential to establish baseline measurements for each scenario to enable accurate comparisons. Initially, measurements were taken with an empty water tank, containing only a free jet. Next, a smooth silicone membrane without denticles was suspended in front of the jet. Finally, to establish a baseline measurement for the single denticle, a plain piece of silicone was mounted on the plexiglass plate.
To ensure that the bristle mechanism is reliably activated by electricity, it is crucial to make the electrical circuit waterproof. This involves taking protective measures to prevent the intrusion of water, which could otherwise cause short circuits or electrical faults. By thoroughly sealing and insulating the circuit components, we can maintain the integrity and functionality of the mechanism. Copper extension wires have been selected to connect the power source outside the water tank, ensuring minimal electrical power loss due to copper's excellent conductivity. To create a watertight connection between the copper wires and the Niti wire, heat shrink tubing has been used. This ensures a secure and waterproof seal,

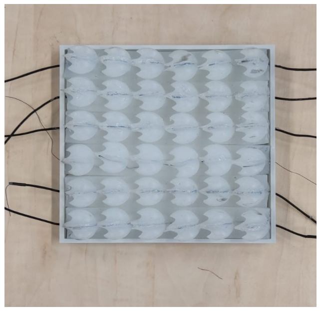

(a) Linearly-overlapped biomimetic sharkskin

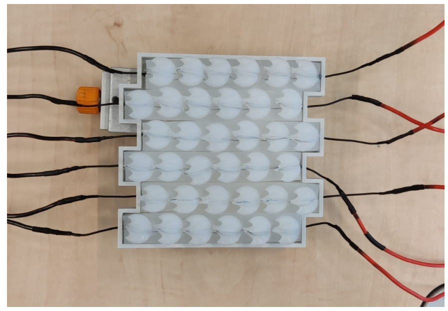

(b) Staggered-overlapped biomimetic sharkskin

(c) Single denticle

Figure 30: Different configurations of shark denticles

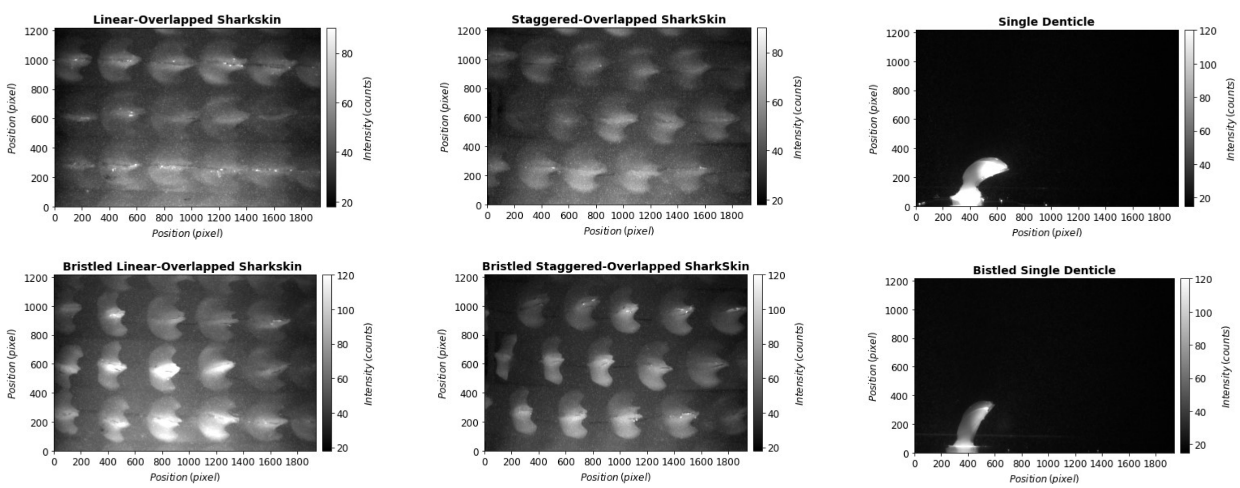

Figure 31: Denticle configurations shown in both resting and bristled states.

protecting the electrical components from moisture and maintaining efficient power transmission.

4.3 Results

Figure 32 presents 9 instantaneous images from the PIV measurements across all different configurations. For these measurements, 1000 double-frame images were captured, with the figure depicting one snapshot of the measurement taken at the midpoint, specifically the 500th image. The first row displays all baseline measurements, the second row illustrates the different configurations without actuation, and the third row shows the same configurations with the denticles actuated. The axes of the graphs, x and y, are normalized by the diameter of the pump's nozzle, which is 6 cm. The Field of View (FOV) is approximately 10 cm by 6 cm. The x-axis starts at 0.25 x/D because the outlet of the pump's nozzle, defined as zero, is located 2 cm upstream from the beginning of the FOV.
The initial data already show some differences between the configurations, especially the single denticle which clearly affects the current. In Figure 33 the average of all PIV measurements depicted. It concerns the average speed of the streamwise flow.

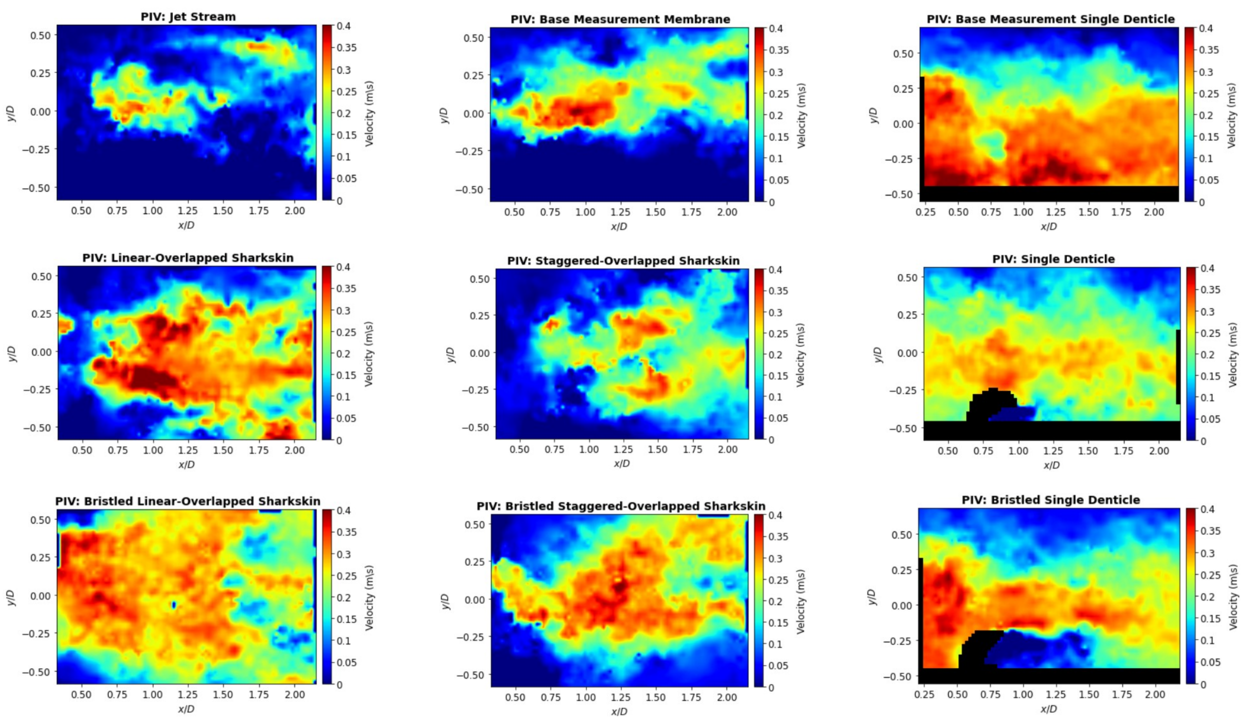

Figure 32: Instantaneous PIV measurement stream-wise velocity in m/s

In both linear and staggered arrangements, the rows of denticles are schematically represented within the graph. This graphical representation illustrates the placement of the denticles, revealing the formation of spots due to the interaction of denticles with light. The actuation of the denticles, as depicted in Figure 31, interferes with the light, leading to observable patterns in the graph.

The observed differences between basic measurement, linear-overlapped, and bristled linear-overlapped configurations present challenges for physical explanation. The primary distinction between the base measurement and the linear-overlapped arrangement could arise from

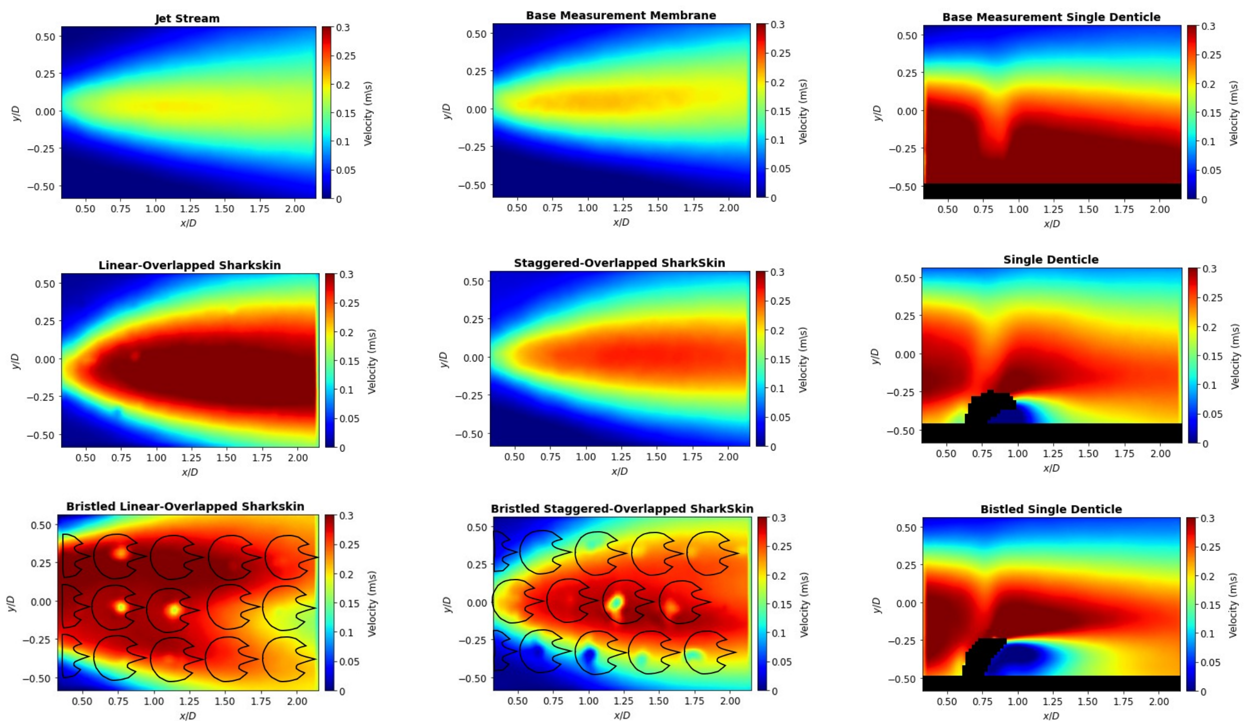

Figure 33: Average stream-wise velocity in x in m/s

the presence of a larger object in front of the pump nozzle. The higher velocities observed in the linear-overlapped configuration can be attributed to the reduced spatial occupation by a membrane without denticles, which consequently diminishes the surface area available for water flow. As the occlusion of this surface area increases, water must flow at higher velocities to maintain the same flow rate. The same applies to the staggered-overlapped and bristled staggered-overlapped. Although there is a noticeable difference between the linear and staggered-overlapped setups, specifically, a narrower current profile and lower speeds with the staggered-overlapped membrane, it is challenging to identify the exact cause of this difference.

In contrast, the differences with the single denticle are more pronounced. Behind the denticle, there is a lower velocity in the x-direction, and the region of influence extends to approximately 0.25 x/D. With the bristled single denticle, this region of influence becomes both larger and longer, extending to about 0.5 x/D. Figure 34 illustrates a simular effect, but focusing on the average speed in the y direction. Here, the blue color indicates a negative (downward) velocity, while red represents a positive (upward) velocity. The bristled single denticle shows a larger red region behind it compared to the denticle at rest. This effect was anticipated, as placing a single object in a stream of water typically produces this result. The images clearly demonstrate the impact of denticle bristling on flow dynamics. A distinct change is observable in the area behind the denticle, suggesting the formation of embedded vortices behind the denticles. In Figure 33, the single denticle column exhibits a dip around 0.75 x/D, observable in all three images. This dip can be disregarded as it is a recurring pattern in all three images. It is likely caused by the shadow generated by the light source shining from below and partially illuminating the silicon because similar to the base measurement, the single denticle is positioned at 0.75 x/D.

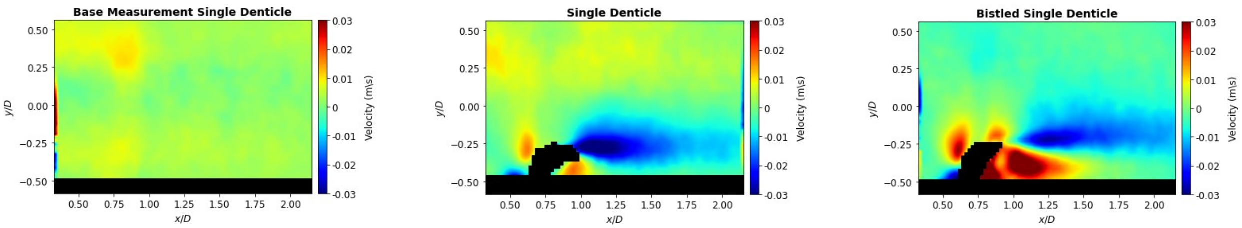

Figure 34: Average velocity in y in m/s

5 Discussion

This thesis explores the fabrication process of biomimetic skin of sharks, focusing on the active control of the bristling effect of denticles observed in the Shortfin Mako shark. By closely examining the natural structure and functionality of shark skin, this research seeks to mimic its unique properties through innovative fabrication techniques.

To create a biomimetic shark skin, various methods previously used to replicate shark skin structures were reviewed and this revealed that an indirect fabrication approach was most suitable. This choice was driven by the necessity to integrate an actuation mechanism into the final design.

Additionally, the design drew inspiration from the field of soft robotics that focuses on creating robots with flexible, adaptable, and deformable structures. In this study, various actuation methods were evaluated, considering their advantages and disadvantages for shark skin design. Nitinol, a shape memory alloy capable of deforming into specific shapes when heated, enabling precise and responsive movements was identified as the optimal choice due to its ability to exert significant force with relatively simple actuation, and its seamless integration into the silicone shark skin.

The material chosen for the biomimetic shark skin is a silicone-based material, specifically Ecoflex 00-10 silicone, selected for its flexibility and workability. This choice ensures that the NiTi wires embedded within the structure can effectively actuate both the membrane and individual denticles.

To create the silicone denticles, a 3D-printed mold was utilized. This mold was printed using Durable Resin V2 on a Formlabs 3B printer. The mold design was crafted in SolidWorks to align six denticles in a row.

The actuation mechanism is versatile, allowing for both global and local adjustments. The global mechanism involves actuating an entire row of denticles to create a predetermined curve, while the local mechanism allows for the angle of individual denticles relative to the skin. By adjusting the design of the mold, the density and arrangement of the denticles can be modified, providing a high degree of customization.

Subsequent experiments involved testing various configurations of biomimetic shark skin in a water tank. Two configurations consisted of a membrane with 6 by 6 denticles, while a third configuration involved testing a single denticle, allowing for different orientations of Particle Image Velocimetry (PIV). The purpose of these tests was to evaluate the performance of the biomimetic shark skin with an integrated actuation mechanism in an aquatic environment. Specifically, the objectives were to determine whether the actuation mechanism would function effectively in water and whether it possessed sufficient power to actuate against the current. Additionally, the tests aimed to investigate potential hydrodynamic advantages, similar to those observed in the Shortfin Mako shark, which enhance swimming efficiency.

The initial findings of this research demonstrate that integrating Nitinol wire actuation mechanisms within a silicone matrix effectively mimics the bristling mechanism, even in aquatic environments. The Nitinol wires exhibit sufficient strength to counteract the water flow induced by the pump, enabling the bristling movement. This confirms that the working mechanism can be reliably tested underwater, within the constraints of the experimental setup.

5.1 Limitations

One notable limitation of this project is the size of the denticles. The rough and uneven skin of the Shortfin Mako shark achieves its drag-reducing function through its micro-roughness. This drag reduction effect diminishes when the denticles become too large, as the increased surface area leads to higher skin friction drag. The design choices for this project were guided by considerations of feasibility and practicality. Consequently, modifications were made to the design in comparison to the original dimensions observed in sharks. In this project, the denticles were enlarged to facilitate the integration of an actuation mechanism. As a result, the denticles of the biomimetic shark skin are approximately 120 times larger than those found on the skin of the Shortfin Mako shark.

The experimental setup had several limitations. Testing the biomimetic shark skins in the water tank necessitated certain modifications. The skin had to be positioned parallel to the LED light to ensure that the camera could capture the illuminated particles. Deviations from this alignment resulted in shadows, rendering the particles invisible. As a result, observations were limited to a top-down view of the denticles. As a result, there was limited visibility into the flow dynamics between and near the denticles. The findings from the Particle Image Velocimetry (PIV) experiment indicate that the denticles and their bristling influence the flow dynamics. However, it remains challenging to ascertain whether this interaction contributes to a reduction in drag.

Additionally, the use of LED light, which produces a broad strip of illumination, caused interference with the denticles. The silicone material, when illuminated by the LED light, exhibited significant brightness, which was reflected as noise in the PIV measurements. This noise was filtered and subtracted using the DaVis software.

In the water tank, only the local mechanism, involving the movement of denticles via the 0.3 mm NiTi wire, was tested. Testing the global mechanism, which is intended to mimic a swimming motion, was impractical. The orientation of the shark skin relative to the LED light meant that any membrane movement would interfere significantly with the light. Although the local bristling effect also posed some interference, it was less pronounced than with the global actuation mechanism. Therefore, it was decided to focus solely on testing the local bristling effect, where only the denticles perform upward movement. Thus, the global mechanism for which the 1 mm NiTi wire actuated the motion was not tested in the water tank.

5.2 Recommendations

Future research focused on accurately replicating the distinct structure found in sharks and incorporating the bristling effect into the design may explore methods for reducing the overall size. This could potentially involve developing alternative materials or techniques to ensure that the denticles remain as close as possible to their original dimensions while incorporating an active bristling mechanism. This approach brings the design closer to nature, potentially creating a refined surface that closely mimics that of the shark.

In this project, 3D printing was employed to create a mold for shaping the intricate form of the denticle. Silicone was then poured into this mold to achieve the desired shape. Future research could explore even more direct manufacturing method, such as advanced 3D printers capable of printing multiple materials interchangeably. This approach would enable the simultaneous printing of materials like metal and polyester, seamlessly integrating an actuation mechanism into the sharkskin and producing a complete structure in one process. Future improvements could include the use of multiple light sources to fully illuminate the entire plane, thereby enhancing visibility between the denticles and utilizing lasers as a light source, as lasers can provide a more focused and narrower strip of light. To address the uncertainty regarding the interaction of denticles and flow dynamics contributing to drag reduction, subsequent research should be conducted in an enhanced testing environment that allows for comprehensive and precise measurement of all relevant effects resulting from the bristling effect of denticles.

6 Conclusion

This thesis investigated the fabrication process of biomimetic shark skin, with a focus on actively controlling the denticle bristle effect, which occurs passively in the Shortfin Mako shark. By closely examining the natural structure and functionality of shark skin, this research aimed to replicate its unique properties through innovative fabrication techniques. The review of various methods previously used to replicate shark skin structures indicated that an indirect fabrication approach was most suitable, driven by the need to integrate an actuation mechanism. Drawing inspiration from the field of soft robotics, the study identified Nitinol, a shape memory alloy, as the optimal actuation material due to its ability to exert significant force with relatively simple actuation and its seamless integration into the silicone shark skin. Subsequent experiments tested various configurations of biomimetic shark skin in a water tank to evaluate the performance of the integrated actuation mechanism. The initial findings demonstrated that Nitinol wire actuation within a silicone matrix effectively mimics the bristling mechanism, even in aquatic environments.

While this research has successfully demonstrated the feasibility of integrating actuation mechanisms into biomimetic shark skin, further studies are necessary to optimize the design for practical applications.

References

Afroz, F., Lang, A., Habegger, M., Motta, P., & Hueter, R. (2017). Experimental study of laminar and turbulent boundary layer separation control of shark skin. *Bioinspiration and Biomimetics*, *12*(1). https://doi.org/10.1088/1748-3190/12/1/016009

Baeten, S. R., Kochovski, A., Jovanova, J., & Sakes, A. (2024). Characterization of shark skin properties and biomimetic replication. *Bioinspiration & Biomimetics*, *19*(5), 051002.

Bengisu, M., & Ferrara, M. (2018). *Materials that move*. Springer International Publishing. https://doi.org/10.1007/978-3-319-76889-2

Bushnell, D. M., & Moore, K. (1991). Drag reduction in nature. *Annual review of fluid mechanics*, *23*(1), 65–79.

Chafik, A. A., Gaber, J., Tayane, S., & Ennaji, M. (2022). Behavioral modeling of knitted shape memory membrane. *2022 XXVIII International Conference on Information, Communication and Automation Technologies (ICAT)*, 1–6.

Dean, B., & Bhushan, B. (2010). Shark-skin surfaces for fluid-drag reduction in turbulent flow: A review. *Philosophical Transactions of the Royal Society A: Mathematical, Physical and Engineering Sciences*, *368*(1929), 4775–4806. https://doi.org/10.1098/rsta.2010.0201

Díez, G., Soto, M., & Blanco, J. M. (2015). Biological characterization of the skin of shortfin mako shark *Isurus oxyrinchus* and preliminary study of the hydrodynamic behaviour through computational fluid dynamics: Hydrodynamics of *isurus oxyrinchus* skin. *Journal of Fish Biology*, *87*(1), 123–137. https://doi.org/10.1111/jfb.12705

Du, Z., Li, H., Cao, Y., Wan, X., Xiang, Y., Lv, P., & Duan, H. (2022). Control of flow separation using biomimetic shark scales with fixed tilt angles. *Experiments in Fluids*, *63*(10), 158. https://doi.org/10.1007/s00348-022-03517-3

Du Clos, K. T., Lang, A., Devey, S., Motta, P. J., Habegger, M. L., & Gemmell, B. J. (2018). Passive bristling of mako shark scales in reversing flows. *Journal of The Royal Society Interface*, *15*(147), 20180473. https://doi.org/10.1098/rsif.2018.0473

Gariya, N., Kumar, P., Prasad, B., & Singh, T. (2023). Soft pneumatic actuator with an embedded flexible polymeric piezoelectric membrane for sensing bending deformation. *Materials Today Communications*, *35*, 105910. https://doi.org/10.1016/j.mtcomm.2023.105910

Graybill, M. T., & Xu, N. W. (2024). Experimental studies of bioinspired shark denticles for drag reduction. *Integrative and Comparative Biology*, *64*(3), 742–752.

Han, X., & Zhang, D. (2008). Study on the micro-replication of shark skin. *Science in China Series E: Technological Sciences*, *51*(7), 890–896.

Khoo, M., & Liu, C. (2001). Micro magnetic silicone elastomer membrane actuator. *Sensors and Actuators A: Physical*, *89*(3), 259–266. https://doi.org/10.1016/S0924-4247(00)00559-8

Kim, U., Kang, J., Lee, C., Kwon, H. Y., Hwang, S., Moon, H., Koo, J. C., Nam, J.-D., Hong, B. H., Choi, J.-B., & Choi, H. R. (2013). A transparent and stretchable graphene-based actuator for tactile display. *Nanotechnology*, *24*(14), 145501. https://doi.org/10.1088/0957-4484/24/14/145501

Koiri, M. K., & Sharma, A. K. (2021). Characterization and behavior study of nitinol shape memory alloy wire for effective and efficient use in soft robotics as an actuator. *Indian Journal of Pure & Applied Physics*. https://doi.org/10.56042/ijpap.v59i3.67755

Kumar Patel, S., Swain, B., Roshan, R., Sahu, N. K., & Behera, A. (2020). A brief review of shape memory effects and fabrication processes of NiTi shape memory alloys. *Materials Today: Proceedings*, *33*, 5552–5556. https://doi.org/10.1016/j.matpr.2020.03.539

Lang, A., Motta, P., Habegger, M., Hueter, R., & Afroz, F. (2011). Shark skin separation control mechanisms. *Marine Technology Society Journal*, *45*(4), 208–215. https://doi.org/10.4031/MTSJ.45.4.12

Lang, A., Habegger, M. L., & Motta, P. (2015). Shark skin drag reduction. In B. Bhushan (Ed.), *Encyclopedia of nanotechnology* (pp. 1–8). Springer Netherlands. https://doi.org/10.1007/978-94-007-6178-0_266-2

Lang, A. W., Bradshaw, M. T., Smith, J. A., Wheelus, J. N., Motta, P. J., Habegger, M. L., & Hueter, R. E. (2014). Movable shark scales act as a passive dynamic microroughness to control flow separation. *Bioinspiration & Biomimetics*, *9*(3), 036017. https://doi.org/10.1088/1748-3182/9/3/036017

Lang, A., Motta, P., Hidalgo, P., & Westcott, M. (2008). Bristled shark skin: A microgeometry for boundary layer control? *Bioinspiration and Biomimetics*, *3*(4). https://doi.org/10.1088/1748-3182/3/4/046005

Lauder, G. V. (2015). Fish locomotion: Recent advances and new directions. *Annual review of marine science*, *7*(1), 521–545.

Livya, E., Sai Anirudh, R., Vignesh, V., Prasannavenkatesh, B., & Nadaraja Pillai, S. (2019). Experimental analysis of implementing roughness on naca 0018 airfoil. *Innovative Design, Analysis and Development Practices in Aerospace and Automotive Engineering (I-DAD 2018) Volume 1*, 91–96.

Lloyd, C., Peakall, J., Burns, A., Keevil, G., Dorrell, R., Wignall, P., & Fletcher, T. (2021). Hydrodynamic efficiency in sharks: The combined role of riblets and denticles. *Bioinspiration and Biomimetics*, *16*(4). https://doi.org/10.1088/1748-3190/abf3b1

Miyazaki, M., Hirai, Y., Moriya, H., Shimomura, M., Miyauchi, A., & Liu, H. (2018). Biomimetic riblets inspired by sharkskin denticles: Digitizing, modeling and flow simulation. *Journal of Bionic Engineering*, *15*, 999–1011.

Motta, P., Habegger, M. L., Lang, A., Hueter, R., & Davis, J. (2012). Scale morphology and flexibility in the shortfin mako isurus oxyrinchus and the blacktip shark carcharhinus limbatus. *Journal of Morphology*, *273*(10), 1096–1110. https://doi.org/10.1002/jmor.20047

Oeffner, J., & Lauder, G. V. (2012). The hydrodynamic function of shark skin and two biomimetic applications. *Journal of Experimental Biology*, *215*(5), 785–795. https://doi.org/10.1242/jeb.063040

Patricia, F.-W., Guzman, D., Iñigo, B., Urtzi, I., Maria, B., & Manu, S. (2019). Morphological characterization and hydrodynamic behavior of shortfin mako shark (isurus oxyrinchus) dorsal fin denticles. *Journal of Bionic Engineering*, *16*(4), 730–741. https://doi.org/10.1007/s42235-019-0059-7

Pu, X., Li, G., & Liu, Y. (2016). Progress and perspective of studies on biomimetic shark skin drag reduction. *ChemBioEng Reviews*, *3*(1), 26–40. https://doi.org/10.1002/cben.201500011

Santos, L. M., Lang, A., Wahidi, R., Bonacci, A., Gautam, S., Devey, S., & Parsons, J. (2021). Passive separation control of shortfin mako shark skin in a turbulent boundary layer. *Experimental Thermal and Fluid Science*, *128*, 110433.

Wang, J., & Chortos, A. (2022). Control strategies for soft robot systems. *Advanced Intelligent Systems*, *4*(5), 2100165.

Wen, L., Weaver, J. C., & Lauder, G. V. (2014). Biomimetic shark skin: Design, fabrication and hydrodynamic function. *Journal of Experimental Biology*, *217*(10), 1656–1666. https://doi.org/10.1242/jeb.097097

Wen, L., Weaver, J. C., Thornycroft, P. J. M., & Lauder, G. V. (2015). Hydrodynamic function of biomimetic shark skin: Effect of denticle pattern and spacing [Publisher: IOP Publishing]. *Bioinspiration & Biomimetics*, *10*(6), 066010. https://doi.org/10.1088/1748-3190/10/6/066010

Zhang, C., Gao, M., Liu, G., Zheng, Y., Xue, C., & Shen, C. (2022). Relationship between skin scales and the main flow field around the shortfin mako shark isurus oxyrinchus. *Frontiers in Bioengineering and Biotechnology*, *10*. https://doi.org/10.3389/fbioe.2022.742437

A Appendix A: Literature study

Literature review

Characterization of shark skin properties and biomimetic replication

]Stan R R Baeten, Delft University of Technology, Mechanical Engineering;
Ana Kochovski; Italian Institute of Technology ;
Dr. Jovana Jovanova, Delft University of Technology, Mechanical Engineering;
Dr. Aimée Sakes, Delft University of Technology, Mechanical Engineering, NWO (Netherlands Organization for Scientific Research) domain AES (Applied and Engineering Sciences)
Email adress Corresponding Author: S.R.R.Baeten@student.tudelft.nl

Abstract

This review explores the present knowledge of the unique properties of shark skin and possible applications of its functionalities, including drag reduction and swimming efficiency. Tooth-like denticles, with varied morphologies, sizes, and densities across the shark's body, significantly influence the flow and interaction of fluids. Examining dermal denticle morphology, this study unveils the functional properties of real shark skin, including mechanical properties such as stiffness, stress-strain characteristics, and denticle density's impact on tensile properties. The adaptive capabilities of the Mako shark scales, especially in high-speed swimming, are explored, emphasizing their passive flow-actuated dynamic micro-roughness. This research contains an overview of various studies on real shark skin, categorizing them into skin properties, morphology, and hydrodynamics. The paper extends exploration into industrial applications, detailing fabrication techniques and potential uses in vessels, aircraft, and water pipes for friction reduction. Three manufacturing approaches, bio-replicated forming, direct fabrication, and indirect manufacturing, are examined, with 3D printing and photo-configuration technology emerging as promising alternatives. Investigations into the mechanical properties of shark skin fabrics reveal the impact of denticle size on tensile strength, stress, and strain. Beyond drag reduction, the study highlights the shark skin's role in enhancing thrust and lift during locomotion. The paper identifies future research directions, emphasizing live shark testing and developing synthetic skin with the help of 3D printing incorporating the bristling effect.

Keywords: Shark skin, Denticles, Drag reduction, Biomimetic replication

1 Introduction

During the evolutionary journey, the shark experienced numerous transformations in key aspects of its anatomy and physiology. These changes encompass adaptations such as acquiring a sleek body shape and the emergence of dermal denticles(Donley et al., 2004). Shark skin has been an interesting source of inspiration for research because of its unique features that make the skin special in multiple ways. The complex resistive structure of shark skin has fascinated physicists, engineers, and biologists for decades. The skin is decorated with tiny denticles in the dermis, often described as tooth-like structures, that extend from the flexible epidermis. These denticles come in different sizes and shapes, depending on their location on the body, and typically have a width of 0.1 mm to 1 mm (Lloyd et al., 2021; Reif, 1978; Reif & Dinkelacker, 1982). One of the functions of the denticles is disrupting the boundary layer of water next to the skin, reducing turbulence around the body and, as a result, reducing resistance during swimming (Díez et al., 2015). This functionality of the shark skin is explained by several components, such as morphology, hydrodynamics, the material properties of the skin, and the locomotion of the shark itself, as the shark's shape dynamically alters the spacing between the denticles. Another remarkable capability of fast-swimming sharks is the bristling effect, an ability to erect each denticle, which has raised the interest of researchers.

The Mako shark (*Isurus oxyrinchus*) is a widely studied species and known as one of the fastest swimmers among sharks. In addition to its streamlined profile, the Mako shark possesses this unique bristling ability that allows it to control the separation of currents, further enhancing its hydrodynamic performance (A. W. Lang et al., 2014).

Understanding these noteworthy features of shark skin has not only provided insights into the evolutionary adaptations of these marine predators but has also ignited interest in the field of biomimetics. Researchers and engineers have sought ways to replicate the drag-reducing properties of shark skin to enhance the design of various applications, from swimming suits to the fuselages of aircrafts (Oeffner & Lauder, 2012; Pu et al., 2016).

In this comprehensive review, we explored the unique properties of the skin of several species of sharks. We delve into the mechanisms underlying the resistance-reducing properties of shark skin and the role of denticles. This review also discusses the underlying principles for the transition from biology to biomimetics and shows how the sharks' blueprints are translated into breakthrough technologies.

Current research has also focused on exploring the multifaceted functionalities of shark skin denticles, as exemplified by Ghimire et al. (2024) recent publication 'Shark Skin Denticles: From Morphological Diversity to Multi-functional Adaptations and Applications.' Although there are overlaps in our research on shark skin properties, such as the recognition of drag reduction and denticle morphology, our research differs in some areas. Ghimire et al. (2024) highlights advances in antifouling studies and bioluminescent adaptations, whereas this research investigates multiple studies that gathered shark skin samples from various locations on the body while delineating the methodology employed.

Overall, this study seeks to answer the following research question:

What is the current state of scientific knowledge regarding the unique properties of shark skin, the diverse testing methodologies utilized to analyse the skin, and the potential interdisciplinary applications such as biomimetic surfaces for ships or aircrafts and materials science?

2 Method

2.1 Systematic search

In the course of this review, a systematic search was conducted on Scopus and ScienceDirect databases utilizing the following search strings:

"Shark AND (skin* OR denticle* OR scale*) AND (drag OR Stiffness OR material*)",

"Shark AND (skin* OR denticle* OR scale*) AND (biomimetic* OR bio-inspir* OR mimic*)" and

"Shark AND (skin* OR denticle* OR scale*) AND (flow* OR morphology OR hydrodynamic*) AND (locomotion OR swim OR movement)."

The search, which included keywords related to shark anatomy, biomimetics, hydrodynamics, and locomotion, resulted in the identification of a total of 509 relevant papers. After an initial review of titles and abstracts, a total of 67 documents were identified that met the criteria for further research. While acknowledging that sharkskin serves purposes beyond drag reduction, such as its antibacterial properties, this review does not delve into these aspects extensively. Additionally, although longstanding bio-inspired riblets are considered, they are not the primary focus, as more attention is given to biomimetic skins that try to recreate the entire denticle shape. Further, a two-step screening process was performed, comprising title and abstract screening and full-text assessment using predefined eligibility criteria:

- The content of the study should provide information about shark skin morphology.
- The study should address the hydrodynamic properties of shark skin.
- The study should provide information about the manufacturing process of the biomimetic shark skin.
- The content of the study should offer a deeper understanding of the characterization methods for shark skin.
- Studies that cover topics beyond drag reduction, such as antibacterial properties, are excluded.
- Studies presenting the longstanding bio-inspired riblets are not the primary focus of this work.

After full-text examination, another 26 papers were excluded, resulting in a refined selection of 41 documents that were considered relevant and were included in this study. The PRISMA flowchart for a systematic review is given below in Figure 1(Page et al., 2021).

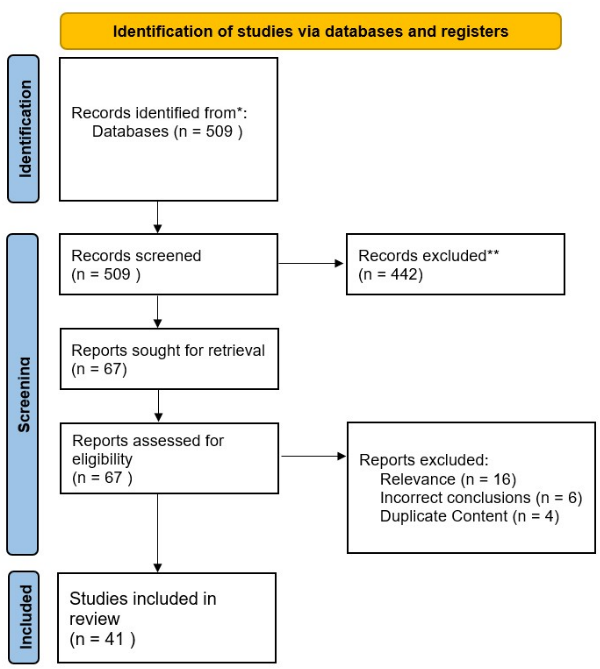

Figure 1: PRISMA flowchart systematic review. Adapted from Page et al. (2021). CC BY 4.0.

3 Structure and properties of biological shark skin

This chapter focuses on the microstructure of the shark skin. When viewed from a distance, shark skin looks like a smooth, streamlined surface designed to swim efficiently. But at the microscopic level tiny structures, known as denticles, encroach on the skin, offer unparalleled insights into the evolution of resistance reduction and hydrodynamics. We discuss and compare the morphology of denticles at different locations on the skin. In addition, we review the stiffness, roughness, and density of the shark skin. Finally, a comparison is made between results from the included studies and an illustration is provided showing the different tests that were performed at different locations on the torso.

3.1 Morphology and size of shark skin denticles

Dermal denticles are an essential part of shark skin's dermal layer. Meyer and Seegers, 2012 state that each denticle is coated with enamel and dentine, which are two distinct tissues found in the structure of teeth. The denticles have a longitudinally oriented pattern of riblets arranged in rows in the same direction as the water flow and contribute to reduced skin resistance(Bushnell & Moore, 1991). In certain places throughout the body, the denticles exhibit ridges exclusively on their leading surface. Even the rounded and widely spaced denticles of some shark species, as shown in Figure 2a, show ridges on their anterior edges. The ridge's height varies depending on the species and the position in the body. The bases of the denticles are extended and firmly anchored to fibers in the lower stratum compactum layer of the dermis (Creager & Porter, 2018). Figure 3 shows four different perspectives of a three-dimensional model of an individual denticle, providing insight into its appearance. Different heights of the ridges are shown, with the central ridge being higher than those on the sides. It is noteworthy that the presented model contains three ridges, which serve as an illustrative example since denticle morphology shows many variations in terms of shape, size, and number of ridges.

Feld et al. (2019) analyzed microscope images of the denticles of a small-spotted catshark. They documented data on the length of selected denticles as well as the total number of denticles present in each frame. Their research revealed that crown lengths for the dermal denticles range from 300 μm to 1 mm. Smaller dermal denticles were predominantly observed on the fins and in close proximity to the gills, while larger dermal denticles were mainly distributed on the body. According to C. Zhang et al. (2022), who conducted research on the Shortfin Mako shark, the length of the denticles ranges between 105 $\pm$ 7 μm and 286 $\pm$ 25 μm and the width of the denticles between 87 $\pm$ 4 μm and 255 $\pm$ 22 μm. The length-to-width ratio ranged from 1.02 to 1.45. In addition, Díez et al. (2015) found that the average height is between 90–110 μm, which includes the height of the peduncle (the base of the denticle) that connects the crown to the skin. Shark denticles, unlike those of other bony fish, do not increase in size as the shark grows. Instead, their structure and size are primarily determined by their growth position and the specific species of the shark (Pu et al., 2016).

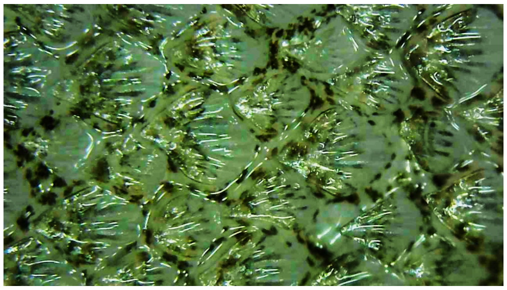

(a) Starry Smouth Hound shark, rounded and widely spaced denticles on top of the head

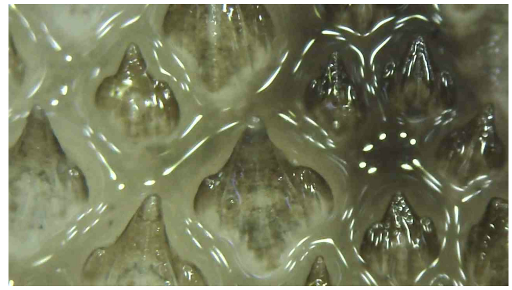

(b) Small Spotted Cat shark, long sharp denticles in front of the dorsal fin

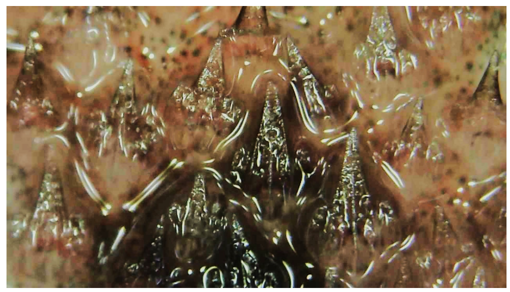

(c) Small Spotted Cat shark, long sharp denticles behind the dorsal fin

Figure 2: Microscopic pictures of structure and arrangement of the denticles of the Starry smoothhound shark and Small Spotted Cat shark

3.1.1 Arrangement and density of shark skin denticles

The structural composition, shape, and density of the denticles of the shark skin show differences among different parts of the shark's body. Figure 2 shows the lattice structures and shapes in different areas of the skin from head to tail of two different species of sharks (Small Spotted Cat shark and Starry smoothhound shark). This figure clearly shows significant differences between species, but also differences within one species since the two pictures of the Cat shark were taken in front of and behind the first dorsal fin, respectively.
According to Díez et al. (2015), the denticle density along both the longitudinal and vertical axes of the Shortfin Mako shark (*Isurus oxyrinchus*) revealed a noteworthy increase in the number of denticles per square millimeter in the dorsal and ventral regions compared to other areas. This density gradually decreased when moving toward the shark's central body, with the lowest density observed along the central longitudinal axis. Additionally, a statistically significant higher denticle density was observed in the anterior region compared to the central region. Towards the posterior region of the shark, the density showed to increase again.

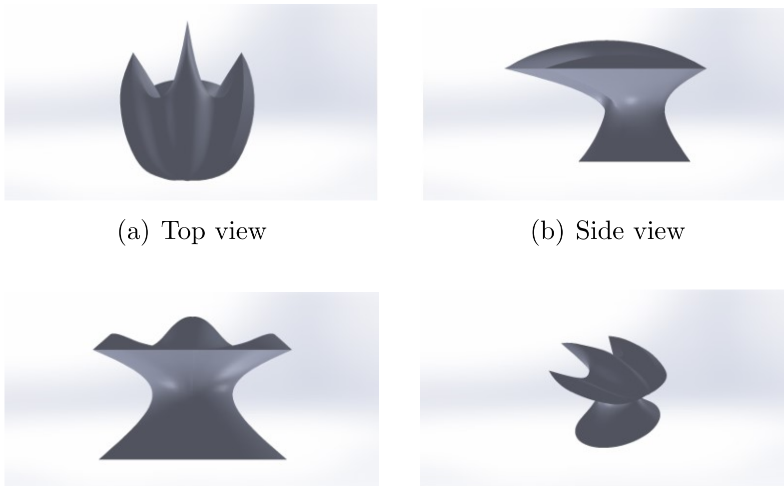

(a) Top view (b) Side view

(c) Front view (d) Iso view

Figure 3: Top, side, front and iso view of a 3D reconstructed model of a single denticle of the shark skin

3.2 Functional properties of shark skin

The versatility of the shark's skin goes beyond its primary role in reducing drag. In addition, the skin serves as an antibacterial barrier and prevents the attachment of marine life to the surface because the placement of the scales alters the turbulent boundary of the water at the surface and generates numerous small eddies as the water flows over the skin. Additionally, another mechanism that may hinder bacterial attachment is super hydrophobia, which results from air trapped in the rough features of the skin, hindering both initial wetting and subsequent attachment(Chien et al., 2020; Zhao et al., 2014). The increased shear stress in this turbulent flow is critical. This fluid dynamic process makes it challenging for benthic diatoms and mussels to attach because the shear stress exceeds their ability to attach (Peng et al., 2009). The shark skin may even offer protection from predators (Creager & Porter, 2018) .

A special feature was documented by Southall and Sims (2003), and they describe a scenario in which a shark species strategically uses its skin structure while feeding in their paper. Juvenile dogfish use dermal denticles to manipulate and process food, attaching it to the lateral-caudal body region. Southall and Sims (2003) named this behaviour pattern scale rasping. These movements keep the food "hooked" in backward-facing denticles, pulling the prey tight.

Another aspect of the skin that has been studied is material properties, including stiffness and how the skin responds to tension and stretch. In a study of Naresh et al. (1997) the stress-strain characteristics of shark skin were analyzed, revealing directional effects in the stress-strain curves. Dumbbell-shaped samples of skinned raw skin were used for testing. The study involved dissection of samples in four different directions: 1) parallel to the longitudinal axis of the shark, 2) perpendicular at a 90° angle to the latitudinal axis, and 3,4) two diagonal directions (at a 45° angle to the longitudinal axis) at two different locations both anterior and posterior. The study used a measurement length of 12 mm, a strain rate of 0.4167 per minute, and an Instron universal tensile bench with a fluid cell. A minimum of 12 samples were tested for each direction at both locations, and average stress-strain curves were plotted, with sample thicknesses ranging from 1.5-2.0 mm. Final stress ranged from 24 to 32 MPa. Parallel samples showed higher strain rates. Regional differences were more apparent in diagonal samples, with posterior samples showing greater stiffness. These differences can be explained by the orientation and curvy or wavy structure of the fibers. When force is applied, a significant portion of that force is used to straighten out these wavy fibers, influencing the material's response to mechanical stress. In the anterior region, the orientation compared to the stress axis is a significant 120°, while the deviation in the posterior region is less pronounced, at 15°.(Naresh et al., 1997).

The study of Creager and Porter (2018) argues that an increase in denticle density will improve the tensile mechanical properties (stiffness, strength, and toughness) of shark skin. Denticle density, measured in number of denticles per square millimeter, was quantified along with quasi-static mechanical properties, including ultimate strength, yield strength, stiffness and toughness, at ten different locations on five different species of shark. The focus was specifically on quasi-static tensile tests-to-failure to determine the ultimate limits of shark skin mechanical properties. Dumbbell-shaped samples of dissected skin were clamped between stainless steel fixtures and were extended in the cranial to caudal direction at a strain rate of 2 mm/s until failure. In Figure 4, the mid-lateral, dorsal, and ventral regions are shown, which are distinguished in a study of Creager and Porter (2018). The study revealed significant differences in ultimate tensile strength (UTS), with the bonnethead shark (Sphyrna tiburo) displaying the highest UTS at 47 MPa in the caudal region (L3) and the lowest at 9 MPa in the ventral region (V2). Other species, including the scalloped hammerhead, Blacktip, bull term embryos, and Shortfin Mako sharks, exhibited the greatest UTS values in the dorsal cranial (D1) region. There were notable species and region effects for stiffness, with the highest stiffness consistently found in the dorsal-cranial (D1) region across all species. Toughness varied significantly among species and regions, with the greatest toughness observed in the cranial (D1) region of Scalloped Hammerhead and Blacktip sharks, caudal (L3) region of Bonnethead sharks and bull term embryos, and dorsal (D3) region of Shortfin Mako. Denticle density did not significantly correlate with ultimate tensile strength, but stiffness increased and toughness decreased with denticle density (Creager & Porter, 2018).

Research on the effect of bristling has discovered that Mako sharks have the ability to finely adjust their scales when swimming at high speeds. This adaptation is rooted in the stratum compactum, which consists of numerous layers of collagen fibers, forming the shark's exoskeleton. This unique structure allows the shark to maintain a balance between longitudinal and hoop stresses, keeping it flexible and storing elastic energy to swim efficiently (A. Lang et al., 2008).

Motta et al. (2012) compared the Shortfin Mako shark and the Blacktip shark and concluded that the scales of the Mako shark are shorter, narrower, and have a shallower ribbing pattern. The scales on the sides of the Mako shark's body are triangular, allowing them to rotate easily around their broad but short base, while the scales on other parts of the body of the Mako shark and those of the Blacktip shark are broader and rhomboid-shaped. The lateral sides of the body, from behind the gills to the tail, have the most flexible scales. It is possible to lift these scales to angles greater than 50° easily, even in dead specimens (A. Lang et al.,

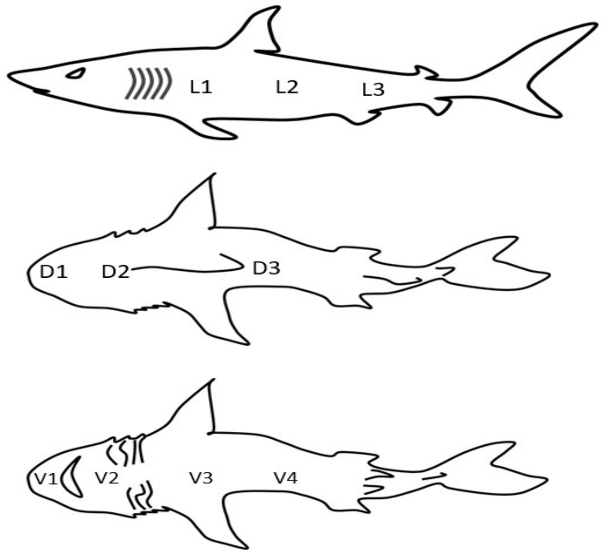

Figure 4: Regions where samples were taken from the mid-lateral (L), dorsal (D) and ventral (V)

2011).

Initially, it was believed that there were multiple ways for the scales to become erect, such as changes in skin tension at higher swimming speeds or the potential for scales to bristle in areas with concave body curvature during swimming (A. Lang et al., 2008). Later on, A. Lang et al. (2014) showed that the scales are able to erect only by the reversal of the water current, without requiring body movement or an active muscular contraction mechanism. As a result, the skin surface of the shark serves as a passive, flow-actuated dynamic micro-roughness. This was also later proven by Du Clos et al. (2018), who analyzed video footage of water flow over the skin of a shortfin Mako shark.

3.3 Roughness and Hydrodynamic properties of shark skin

In order to gain a more detailed understanding of the exact morphology of a denticle, Ankhelyi et al. (2018) has performed research on skin samples at 20 different locations on the body of the Dusky smoothhound shark (*Mustelus canis*). The study involved calculating metrology variables, including roughness (Sq), skew (Ssk), kurtosis (Sku), and max height (Sz), for entire sample images of three individual smoothhound sharks. Additionally, the average length and width of three denticles for each region on each individual shark were measured. Spacing between adjacent denticle ridges and denticle ridge height for five denticles on one individual were also measured. Skew values above or below zero signified more peaks or valleys, respectively. Kurtosis values above three indicated surfaces with high peaks and low valleys, while values below three suggested less extreme surface variation. To provide an idea of the range of profilometry variables, Table 1 shows the minimum and maximum values of all the different variables.

The maximum of the average length and width of a denticle was at the tip of the shark's

Table 1: Summary of Profilometry data

Variable	Maximum	Minimum
Sq (mm)	42.1	3.5
Ssk	20.86	20.25
Sku	8.2	2.8
Sz (mm)	323.3	38.0
Average Length (mm)	554.7	125.9
Average Width (mm)	459.6	126.6

nose, while the minimum of both is just behind the pectoral fin. The highest roughness was measured just before the first dorsal fin, and the lowest value of roughness was measured behind the pectoral fin.

When a shark swims, it encounters two primary sources of drag: 1) skin friction drag and 2) form drag (A. Lang et al., 2015). Skin friction drag, arising from the friction between water and the shark's body, is associated with the flow moving over the shark. This type of drag results from the no-slip boundary condition between the water and the shark, forming a boundary layer. High swimming speeds result in a high Reynolds number, leading to turbulent flow across the shark's body and a substantial increase in skin friction. The second type of drag, form drag, is more crucial to control. It originates from pressure differences around the body and depends on whether the flow remains attached or separates during swimming (A. Lang et al., 2015). The water flow experiences a favorable pressure gradient from the nose to the point of maximum girth (near the gills), while unfavorable pressure gradients occur downstream of this point, causing a substantial increase in drag. (A. Lang et al., 2011). This aligns with the observation that for the fast-swimming Mako shark, the most flexible scales are situated on the body's flanks and downstream of the gills, regulating flow separation (A. Lang et al., 2011).

The study of Miyazaki et al. (2018) discusses the morphology of a single denticle of the Galapagos shark and highlights a structure with five ridges and four grooves. This feature, referred to as non-uniform grooves in the study, is defined by distinct differences in height or spacing between the ridges on top of the denticle. The research observes strong longitudinal vortices concentrating at the ridges of shark skin denticles, particularly near the side ridges. Weak longitudinal vortices are noted in the valley of the grooves, suggesting that the multiple-ridge denticles play a role in disrupting longitudinal vortices and weakening secondary flows. This disruption may isolate high shear stress across the grooves, reducing the exposure of a significant portion of the denticle surface to high mean shear. The non-uniform grooves, specifically the unique five-ridge denticles, are highlighted for their morphological significance in passive flow control near shark skin. A systematic Computational Fluid Dynamics (CFD) study explores how the morphology of multi-sharp-ridge denticles, characterized by non-uniform grooves, affects passive turbulent flow control (Miyazaki et al., 2018). The investigation focuses on the hydrodynamic effects of height-to-spacing ratios of mid-ridge and side-ridges. The study found that an increase in non-uniform height-to-height and spacing-to-spacing ratios enhances the strength of longitudinal vortices, clarifying how non-uniform grooves enhance secondary flows better than uniform grooves.

Overall, the results of the study of Miyazaki et al. (2018) confirm the morphological significance of multiple-ridged non-uniform grooves in passive turbulent flow control near shark skin denticles.
As mentioned before, the Shortfin Mako shark has loosely anchored denticles across its body that, through a flow-activated mechanism, can control the separation of the flow, thereby reducing resistance (Patricia et al., 2019). The study of Afroz et al. (2017) tested the skin of Shortfin Mako sharks, specifically from the flank region with highly movable scales, under various adverse pressure gradients (APG) to assess its ability to control separation in fluid flow. The results showed that shark skin can effectively control both laminar and turbulent separation on a flat, non-moving surface. Furthermore, the presence of shark skin on the flat plate resulted in a smaller separation region and a delayed separation point under different magnitudes of APG. Santos et al. (2021) even compared different bristling angles observed at the Mako shark, including 50 degrees and 30 degrees. The results indicated that denticles with a 50-degree angle were most effective in reducing and possibly eliminating flow separation.

3.4 Insights into shark skin research: Samples, methodologies, and species diversity

Figure 6 illustrates the location where the skin samples were taken, and the color indicates what research was done. A distinction is made between research focused on skin properties (red), morphology (yellow), and hydrodynamics (blue). These are the three main areas of research shown in Table B in Figure 6. In Table C, the various studies that have investigated real shark skin are listed. Unfortunately, not all studies mentioned the body location, providing only the quantity of samples taken. Some studies have been executed at the same location. In total 21 studies were included and compared. Upon examining the shark and the areas under research, it becomes evident that extensive research has been done on the fins and tail area, focusing on morphology and hydrodynamics. These aspects also contribute significantly to locomotion and maintaining stability for the fin area and to thrust for locomotion for the tail area. Furthermore, it is evident that the studies which examined the properties of the skin were exclusively conducted on the mid-lateral area (L1, L2, L3).
In all of the 21 studies, a total of 19 different species of sharks were examined. The Shortfin Mako shark was by far the most frequently sampled, with the Blacktip and Hammerhead sharks in second and third place, respectively. With over 10 studies having collected samples of the Mako shark, researchers have extensively investigated the distinctive characteristics of this shark species. Shark samples are typically preserved by freezing or immersing them in a solution with a high ethanol percentage to ensure proper preservation. Two papers utilized freshly dead samples. However, no studies were conducted on live animals.
To determine the morphology of denticles, scanning electron microscopy (SEM) and gel-based profilometry together with micro-CT imaging are consistently used to create 3D maps of denticles, which help in their detailed analysis.
Hydrodynamic analysis is usually performed using two distinct methods. Particle image velocimetry (PIV) is an optical measurement technique used in fluid mechanics to visualize

and quantify the flow patterns and velocities of fluids to assess the hydrodynamics of the denticle in a given setup. Alternatively, computer models, primarily using computational fluid dynamics (CFD), which employs numerical methods and algorithms to simulate and analyze the behavior of fluid flows around the denticle, were used. Tensile tests were conducted using hourglass-shaped or dumbbell-shaped specimens to assess the tensile strength, stress, and strain of the skin.

4 Biomimetic shark skin

4.1 Fabrication methods towards replicating shark skin

Imitating shark skin offers many advantages across diverse industrial sectors, including applications in vessels, aircraft, and the interior of water pipes for friction reduction (Bixler & Bhushan, 2013; Domel et al., 2018b; Ibrahim et al., 2018). Different methods are available for manufacturing these replicas. This section explores various fabrication techniques and considers potential applications. Additionally, the performance of different bio-inspired surfaces will be explored and analyzed.

The majority of the existing studies on shark skin-inspired low-drag surfaces fall into the following categories: (1) simplified structures with rectangular or triangular line patterns such as riblets, (2) direct replication or 3D printing of biological shark skin (Jo et al., 2021). Different techniques for manufacturing biomimetic shark skin are discussed by Pu et al. (2016). Three primary approaches are examined: 1) the bio-replicated forming method, 2) the direct fabrication of surface microstructures, and 3) the indirect fabrication of surface microstructures.

The bio-replicated forming method replicates surface microstructures using real biological surfaces as templates, as shown schematically in Figure 5a. The negative mold is made by pouring a polymer over real shark skin. Subsequently, a polymer is poured over the negative mold to create a realistic shark skin replica (Han & Zhang, 2008; Pu et al., 2016). Although this method is effective for high fidelity to biological templates, it is constrained by limited resources and cost, making it unsuitable for large-scale applications.

The direct fabrication method constructs microstructures without a negative template and instead uses techniques such as surface machining to create the biomimetic samples as shown in Figure 5b. Although this method offers competent designs, it is generally limited to small-area applications due to cost and efficiency limitations.

The indirect manufacturing method is applied with techniques such as grinding. This indirect manufacturing method also makes use of a negative mold, which captures a shape or form of the object in a reversed or negative way, as shown in 5c. In contrast to the bio-replicated forming method, this technique directly fabricates the negative mold itself instead of casting a polymer over an existing biological template.

Both Pu et al. (2016) and L. Wen et al. (2014) highlight the advantages of 3D printing for making skin models of sharks, compared to traditional manufacturing methods such as computer-controlled CNC milling or casting. The speed of 3D printing allows for fast and efficient creation of large synthetic membranes. Additionally, 3D printing enables the combination of materials with different mechanical properties, such as embedding rigid bio-mimetic

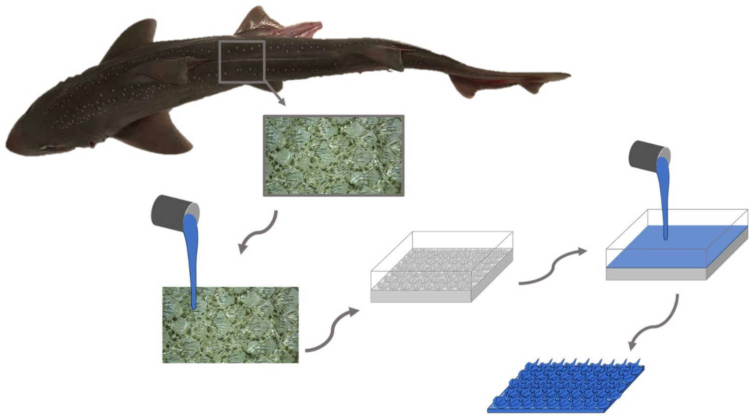

(a) Bio-replicated forming

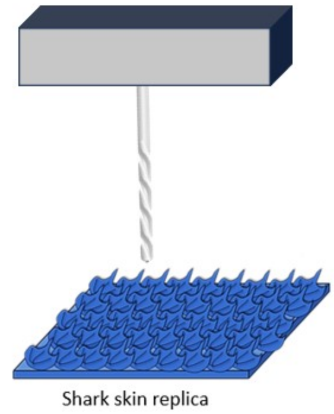

(b) Direct fabrication method

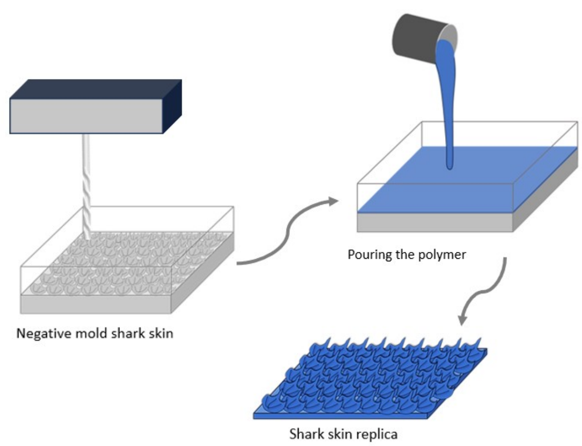

(c) Indirect fabrication method

Figure 5: Basic principle of techniques for manufacturing biomimetic shark skin

denticles in flexible membranes. Unlike techniques such as casting, 3D printing offers control over specific denticle parameters, including size, morphology, spacing, distribution pattern, and mechanical properties (L. Wen et al., 2014). Literature addresses the significant challenge of using 3D printing to replicate the overlapping and overhanging structural features of real shark skin denticles, which is not possible with casting or simple mechanical fabrication procedures (L. Wen et al., 2014). However, performing 3D printing on the actual scale of the shark denticles while maintaining the full surface complexity of natural denticles is still limited.

To overcome the limitations of conventional fabrication approaches, as well as 3D-printing, the photoreconfiguration was developed and first mentioned by Jo et al. (2021). This technique provides a way to create complex and biomimetic structures at the micrometer scale. The process consists of two steps: 1) forming an array of tiny pillars using a mold, and 2) photo reconfiguration of the micropillars, which changes the shape of these pillars. Initially,

a soft mold is produced to shape the azopolymer, which results in the formation of an array of micropillars that serves as the basis for the subsequent structure. The micropillars created in the first step are then modified through a photoconfiguration process. This involves exposing the azopolymer to slant irradiation using the interference light produced by two circularly polarized lights. This specific type of illumination causes the micropillars to undergo a transformation, creating an asymmetric riblet geometry on top of the structure (Jo et al., 2021). The overall goal of this fabrication technique is to replicate the unique surface features found in shark skin that contribute to reduced drag.
J. Wen et al. (2023) investigated the mechanical properties of shark skin fabrics with different denticle sizes, focusing on (a) tensile strength, (b) Young's modulus, and (c) breaking elongation. They produced the fabric with the help of a Form3 3D printer. The printer employed a photopolymerization method to create the intricate microstructure of shark skin fabric. The Form3 printer has a high resolution of 25 microns on the X and Y axes, ensuring detailed replication of shark denticles. The printing involved simultaneous fabrication of the fabric and denticles using Flexible 80A resin, an acrylate-based material compatible with most photopolymerization 3D printers. In the horizontal direction, the fabric with small denticles exhibited the highest tensile strength, measuring 8.73 MPa. Increasing denticle size by 50 % led to a 29.67 % decrease in tensile strength (6.14 MPa). A 20 % increase in denticle size resulted in an 18.35 % decrease (7.52 MPa to 6.14 MPa) (J. Wen et al., 2023). Conversely, in the lengthwise direction, fabric with medium denticles had the highest tensile strength and breaking elongation. The medium denticle fabric showed a 7.17 % increase in elongation at break compared to small denticles, while the large denticle fabric exhibited a 19.07 % decrease. In the horizontal direction, the fabric with small denticles had the highest elongation at break, indicating their potential to enhance breaking elongation in this orientation. These findings highlight the influence of denticle size on the mechanical characteristics of shark skin fabrics, providing valuable insights for applications in material engineering and biomimetic design.

4.2 Applications of biomimetic shark skin

Current engineering applications often use simplified riblet structures inspired by the shark skin. The application of riblet structures shows promise in diverse fields, ranging from maritime to aerodynamics or fluid dynamics in pipes, offering potential improvements in efficiency and performance.
Researchers aim to simplify denticle morphology to create cost-effective and feasible riblet structures for mass applications. For instance, in the aircraft industry, a reduction in fuel consumption of up to 3 % has been achieved by applying a riblet structure on 70 % of the surface area (Pu et al., 2016). For pipe flow engineering, riblet-structured surfaces have been employed for drag reduction in pipe flow and have proven at least a 5 % resistance reduction (Pu et al., 2016). While all riblets share similar functionality, their drag-reduction effectiveness varies based on geometry. For instance, a review of Bechert et al. (1997) revealed that blade-type riblets exhibit the highest drag reduction, reaching up to 9.9 %, compared to scalloped and sawtooth riblet types.
Despite efforts to create 3D riblets with features resembling actual shark skin, experiments of Dean and Bhushan (2010) with staggered segmented-blade riblets failed to achieve greater

drag reduction than optimum continuous blade riblets. The conclusion drawn is that three-dimensional riblets composed of segmented two-dimensional riblets are unlikely to significantly outperform continuous two-dimensional riblets.

The research of Domel et al. (2018b) explored other variations inspired by shark denticles. The experimentation involved testing these variations on an airfoil, considering three distinct shapes. The first shape closely replicated the shark denticle, the second resembled more of a 2D bump that slopes up and then gradually smoothens back down, and the third combined elements from both the shark denticle and the 2D bump, a continuous shark-inspired profile (Domel et al., 2018b). The experiments involved passing air over the airfoil and measuring the outcomes at various angles of attack. Additionally, the lift-to-drag ratio was calculated to assess performance.

The continuous shark-inspired profile outperformed the 2D bump profile and shark denticle in terms of lift-to-drag ratio across various angles of attack (Domel et al., 2018b).The continuous shark-inspired profile showed the lift benefits at low angles and maintained these advantages at higher angles, unlike the 2D bump. Additionally, it significantly reduced drag at higher angles, similar to the shark denticle. The continuous shark-inspired profile exhibited the greatest improvement at the angle of maximum lift-to-drag ratio. Unlike other foils, it overcame the obstacle of structural complexity associated with replicating shark denticles, making it easily adaptable for large-scale production. This advancement enhances the potential adoption of the technology in aquatic and aerospace applications. The study emphasizes that the flow regime examined (Reynolds $\approx 4{\times}10^4$) is applicable to various systems, such as interior sections of wind turbine blades, helicopter blades, drones, and autonomous underwater vehicles. Additionally, the mechanisms identified in this study could be relevant for higher flow regimes, offering potential enhancements for movement through air and water (Domel et al., 2018b).

The study of Dean and Bhushan (2010) found that vortices above riblets mostly interact with the tips, causing localized high-shear stresses. The valleys between riblets have lower shear stresses across most of the surface. Because the vortices are located above the ends of the riblets, the shear stress decreases, reducing the effect of a larger surface area. Although some secondary vortices enter the riblet valleys, their flow results in a small rise in shear stress (Bechert et al., 1986; Dean & Bhushan, 2010). This phenomenon was further demonstrated by Miyazaki et al. (2018), indicating that non-uniform grooves enhance secondary flows better than the commonly used uniform grooves

Ibrahim et al. (2018) performed a numerical analysis of design modifications with biomimetic shark skin to show potential improvements for both rectangular and container ship models. The modifications result in a reduction in wall shear stress, a 3.75 % reduction in resistance coefficient, and a 3.89 % reduction in resistance force for the container ship model. Encouraged by these findings, the study suggests further validation through experimental procedures to increase the impact of this research on the global shipping and maritime industry.

4.3 Hydrodynamic function of biomimetic shark skin

In the study of Oeffner and Lauder (2012), a robotic flapping foil device was employed to assess the impact of shark skin surface features and two biomimetic surfaces on self-propelled swimming speed. The device, designed for studying fish-like propulsion, enabled accurate measurement of swimming speeds, controlled motion programs, and flow quantification using digital particle image velocimetry. Rigid and flexible foils were created from fresh shark skin and two manufactured biomimetic shark skins. The study aimed to test the hypothesis that denticles enhance swimming speed by comparing against a control condition with reduced or absent denticles.

In this context, the study used self-propelling foils that swam under a specific motion program that imitated their natural movement. The study compared the measured surface curvatures of flexible shark skin foils with those observed in live sharks swimming in a laboratory flow tank. The results showed that the foils' curvature values (0.17–0.25 cm^{-1}) aligned well with measured maximal mid-body values from live spiny dogfish (Oeffner & Lauder, 2012). This indicates that when self-propelling, the shark skin membranes bend to a similar extent as the skin of a live shark during unrestrained locomotion.

The study suggests that the effect of skin denticles on shark skin goes beyond drag reduction and plays a crucial role in enhancing thrust. While existing literature has predominantly focused on drag reduction, the denticles are found to alter vortex location. This effect, especially on the tail surface where flow separation and vortex formation occur, could potentially increase thrust rather than solely reducing drag. The findings propose that similar effects of denticles could enhance lift and maneuvering forces on pectoral fins, where vortices are generated during maneuvering (Oeffner & Lauder, 2012).

The study of L. Wen et al. (2014) used a robotic system to evaluate how biomimetic shark skin affects swimming performance. The three main findings of this study were: (1) Biomimetic shark skin showed a maximum reduction of 8.7 % in static drag at lower current speeds but showed increased drag at higher speeds. (2) During swimming, biomimetic shark skin provided a speed increase of up to 6.6 % and a reduction in energy consumption of up to 5.9 % under most kinematic conditions. (3) In particular, compared to a smooth film, the 3D printed shark skin film generated an improved Leading Edge Vortex (LEV). The study highlights the nuanced influence of sharkskin characteristics on swimming performance and highlights the need to consider specific exercise programs to understand the benefits of biomimetic shark skin.

L. Wen et al. (2015) performed a study that aimed to evaluate the effect of denticle arrangement on the swimming performance of biomimetic shark skin using three different denticle patterns: 1) the staggered-overlapped, 2) the linear-overlapped and 3) the linear-non-overlapped array. The researchers used multi-material additive manufacturing to print rigid denticles on flexible panels, assembling them into two-layer membranes for testing. Static drag and dynamic swimming tests were conducted to understand the functional significance of denticle arrangements. The study analyzed the effects of changing denticle arrangement and spacing on swimming performance. The results showed that the linearly-non-overlapped pattern exhibited the slowest swimming speeds, while the staggered-overlapped pattern outperformed others, showing nearly 20 % faster speeds on average despite having a larger total surface area (L. Wen et al., 2015). This suggests that denticle arrangement plays a crucial role in enhancing swimming performance.

Domel et al. (2018a) investigated the influence of denticle size on the performance of biomimetic shark skin. Using 3D printing, model membranes with varying denticle sizes were created, and static tests were conducted to assess drag forces at different flow speeds. Dynamic tests were performed to examine the relationship between denticle size and power consumption during self-propulsion. Results indicate that smaller denticles, particularly at higher self-propelled speeds, lead to improved swimming performance with lower power consumption. Despite the increased surface area of foils with denticles, certain motion parameters, including pitch and frequency, and denticle size combinations contribute to enhanced swimming (Domel et al., 2018a). However, limitations include constraints on accurately 3D printing small shark denticles and flexible membranes. Due to the impracticality of printing shark denticles at their actual size, this study effectively produced a synthetic skin with a surface roughness (Sq) 10 times that of the Shortfin Mako shark.

Bechert et al. (2000) investigated the bristling effect observed in the skin of Mako sharks. They tested the biomimetic skin in an oil channel, which allowed them to magnify the microscopic features of biological shark skin by a factor of 100 due to the viscosity of the oil. This method allowed for the precise reproduction of the intricate shape of shark scales, their flexible attachment, and the variable angle at which the scales are positioned. The experiments revealed interesting results, showing that closely spaced scales with minimal gaps modestly reduced shear stress. However, the synthetic sharkskin replica did not exceed the effectiveness of optimized two-dimensional ribbed surfaces in reducing shear stress (Bechert et al., 2000).

4.4 Future research and innovations

While significant research has already been conducted on shark skin, continuing research will enhance our understanding and potentially provide new insights. Bio-inspired shark skins are currently being implemented, and they are already showing progress despite the fact that they do not replicate the full complexity of a denticle. There are still research gaps that need to be addressed to expand these developments. The researchers who analyze real shark skin rely solely on samples collected from deceased sharks. Although the skin of a dead shark undoubtedly still possesses several distinctive characteristics, in a live shark, other components may play a role, such as muscle stiffness, that may contribute to overall dynamics. Measuring the tension that the skin experiences while swimming is a challenging task with real sharks, but it is a fascinating way to gain valuable insights.

Future research could include a broader range of shark species in the studies that examine the locomotion of sharks and thereby test the influence of distance, pattern, or size of denticles on the drag and dynamic motion of the shark. Different species exhibit variations in denticle patterns, sizes, and arrangements, influencing their hydrodynamic performance differently. Understanding how these factors interact can provide a more nuanced understanding of their combined impact on drag reduction and dynamic motion.

Although there has been research focusing on the bristling effect of the Shortfin Mako shark, still a variety of questions remain. Currently, while efforts have been made to mimic the bristling effect, further research is still required to fully replicate this phenomenon and its effect on thrust generation. A biomimetic skin that can effectively mimic the bristling effect may illustrate many hydrodynamic benefits.

With 3D printing constantly undergoing new developments, achieving an increasingly refined replica of shark skin is within reach. The potential for multi-material 3D printing further enhances the feasibility of creating a biomimetic skin with the characteristics described above. The application of advanced printing techniques will ultimately facilitate the replication of the intricate structure, especially the scale of denticles, to successfully mimic their complexity. Furthermore, recent advances in deep machine learning are poised to revolutionize Computational Fluid Dynamics (CFD) (Runchal & Rao, 2020). This innovation is expected to improve the speed, accuracy, and user-friendliness of CFD software. Runchal and Rao (2020) discusses that deep machine learning will play an important role in creating digital twin and reduced order models, changing the way CFD is applied.

5 Discussion

The microscopic examination of shark skin reveals dermal denticles, tooth-like structures coated with enamel and dentine arranged in rows along the skin. These denticles vary in size, shape, and density depending on their location on the shark's body. The evolutionary significance lies in their ability to disrupt the boundary layer of water next to the skin, reducing turbulence during swimming. Different species and regions of sharks exhibit variations in denticle morphology, with differences in the length, width, and density of denticles contributing to their unique hydrodynamic properties. The arrangement and structure of denticles, as seen in the microscopic examination, play a crucial role in disrupting flow patterns and reducing drag. Studies employing CFD shed light on the disruption of longitudinal vortices by multi-ridged non-uniform grooves, contributing to passive turbulent flow control. The research emphasizes the significance of flexible scales in regulating flow separation, particularly in regions prone to unfavorable pressure gradients. This bristling effect observed in Mako sharks demonstrates the adaptability of the shark's skin to different flow conditions and its ability to erect denticles passively in response to flow reversal, without requiring movement of the body.

The review extends to the material properties of shark skin, including stiffness, strength, and toughness. Research suggests that denticle density did not significantly correlate with ultimate tensile strength. However, an increase in denticle density was associated with higher stiffness and reduced toughness. Understanding the stress-strain characteristics and tensile mechanical properties provides insights into the design of biomimetic shark skin.

The exploration of biomimetic shark skin for various industrial applications, including vessels, aircraft, and water pipes, holds significant promise. The diverse fabrication methods include bio-replicated forming, direct fabrication of surface microstructures, and indirect fabrication of surface microstructures. Each approach has its advantages and limitations, influencing factors such as cost, efficiency, and scalability for large-scale applications. The ability of 3D printing to create intricate structures with specific denticle parameters is highlighted, allowing for control of the size, morphology, spacing, and mechanical properties. Efforts to simplify denticle morphology for cost-effective and feasible mass applications are evident in various studies exploring different riblet structures. Blade-type riblets, in particular, have been identified as exhibiting the highest drag reduction. The continuous shark-inspired profile, combining elements from both the shark denticle and a 2D bump, outperforms traditional profiles in terms of lift-to-drag ratio improvements across various angles of attack. Notably, this profile overcomes structural complexity issues associated with replicating shark denticles, making it adaptable for large-scale production. The impact of shark skin features on swimming performance is discussed, and these studies investigate the influence of shark skin on self-propelled swimming speed, drag reduction, and energy consumption. The findings suggest that shark skin not only reduces drag but also plays a crucial role in enhancing thrust during swimming.

6 Conclusion

The comprehensive review of shark skin properties reveals a fascinating interplay of morphology, hydrodynamics, and material properties. The evolutionary adaptations of shark skin, particularly the role of dermal denticles, provide insights into nature's solutions for drag reduction and efficient swimming. The diverse morphological variations in denticles, coupled with their impact on hydrodynamics, present a rich field for interdisciplinary research. The current state of scientific knowledge highlights the intricate details of shark skin, from microscopic structures to macroscopic adaptations, contributing to breakthroughs in technology and materials science.

Biomimetic shark skin presents a promising avenue for reducing drag and enhancing performance in various applications. The choice of fabrication methods, particularly the utilization of 3D printing, showcases advantages in terms of efficiency, flexibility, and control over denticle parameters. However, challenges remain, such as the need for technological advancements to replicate the intricate morphology of shark skin at biological scales. The implementation of the simple riblet structures, inspired by shark skin, already shows significant potential for resistance reduction and improved efficiency. In locomotion studies, the impact of shark skin on swimming speed and thrust enhancement is evident. Beyond drag reduction, shark skin denticles alter vortex location, potentially increasing thrust and playing a crucial role in lift and maneuvering forces. To summarize, biomimetic shark skin, with its various applications and ongoing advancements in fabrication and understanding its impact on performance, holds great promise for revolutionizing various industries and contributing to more efficient and sustainable technologies.

Appendix

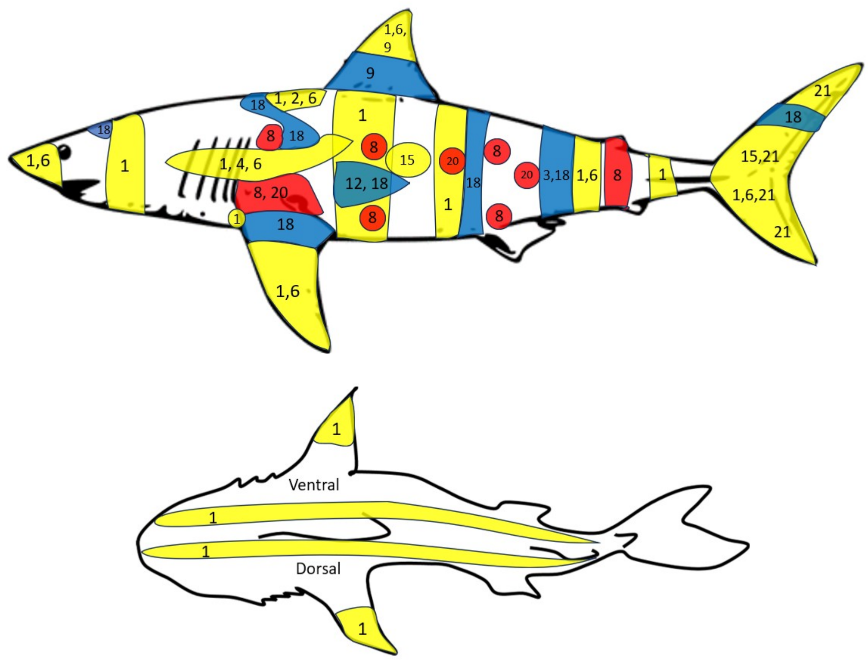

A: Image of locations shark skin samples

Skin properties	Morphology	Hydrodynamics
8,19,20	1,2,4,6,15,16,21	3,5,7,9,10,11,12,13,14,17,18

B: Number of study that conducted research in that section

1	(Díez et al., 2015)	12	(Du Clos et al., 2018)
2	(A. W. Lang et al., 2008)	13	(Luo et al., 2015)
3	(Du et al., 2022)	14	(C. Zhang et al., 2022)
4	(M. Gabler-Smith et al., 2021)	15	(M. K. Gabler-Smith & Lauder, 2022)
5	(Feld et al., 2019)	16	(Motta et al., 2012)
6	(Ankhelyi et al., 2018)	17	(A. Lang et al., 2015)
7	(Afroz et al., 2017)	18	(A. Lang et al., 2011)
8	(Naresh et al., 1997)	19	(Wainwright et al., 1978)
9	(Patricia et al., 2019)	20	(Creager & Porter, 2018)
10	(A. W. Lang et al., 2014)	21	(Popp et al., 2020)
11	(D.-y. Zhang et al., 2011)	-	-

C: Table of various studies

Figure 6: A: Locations where samples were taken for the various studies that investigated skin properties, morphology or hydrodynamics. B: Number of study that conducted research in that section. C: Various studies that investigated skin properties, morphology or hydrodynamics

References

Afroz, F., Lang, A., Habegger, M., Motta, P., & Hueter, R. (2017). Experimental study of laminar and turbulent boundary layer separation control of shark skin. *Bioinspiration and Biomimetics*, *12*(1). https://doi.org/10.1088/1748-3190/12/1/016009

Ankhelyi, M. V., Wainwright, D. K., & Lauder, G. V. (2018). Diversity of dermal denticle structure in sharks: Skin surface roughness and three-dimensional morphology. *Journal of Morphology*, *279*(8), 1132–1154. https://doi.org/10.1002/jmor.20836

Bechert, D., Bartenwerfer, M., Hoppe, G., & Reif, W.-E. (1986). Drag reduction mechanisms derived from shark skin. *IN: ICAS*, *2*, 1044–1068.

Bechert, D., Bruse, M., Hage, W., & Meyer, R. (2000). Fluid mechanics of biological surfaces and their technological application. *naturwissenschaften*, *87*, 157–171.

Bechert, D., Bruse, M., Hage, W. v., Van der Hoeven, J. T., & Hoppe, G. (1997). Experiments on drag-reducing surfaces and their optimization with an adjustable geometry. *Journal of fluid mechanics*, *338*, 59–87.

Bixler, G. D., & Bhushan, B. (2013). Fluid drag reduction with shark-skin riblet inspired microstructured surfaces. *Advanced Functional Materials*, *23*(36), 4507–4528. https://doi.org/10.1002/adfm.201203683

Bushnell, D. M., & Moore, K. (1991). Drag reduction in nature. *Annual review of fluid mechanics*, *23*(1), 65–79.

Chien, H.-W., Chen, X.-Y., Tsai, W.-P., & Lee, M. (2020). Inhibition of biofilm formation by rough shark skin-patterned surfaces. *Colloids and Surfaces B: Biointerfaces*, *186*, 110738.

Creager, S. B., & Porter, M. E. (2018). Stiff and tough: A comparative study on the tensile properties of shark skin. *Zoology*, *126*, 154–163. https://doi.org/10.1016/j.zool.2017.10.002

Dean, B., & Bhushan, B. (2010). Shark-skin surfaces for fluid-drag reduction in turbulent flow: A review. *Philosophical Transactions of the Royal Society A: Mathematical, Physical and Engineering Sciences*, *368*(1929), 4775–4806. https://doi.org/10.1098/rsta.2010.0201

Díez, G., Soto, M., & Blanco, J. M. (2015). Biological characterization of the skin of shortfin mako shark *Isurus oxyrinchus* and preliminary study of the hydrodynamic behaviour through computational fluid dynamics: Hydrodynamics of *isurus oxyrinchus* skin. *Journal of Fish Biology*, *87*(1), 123–137. https://doi.org/10.1111/jfb.12705

Domel, A. G., Domel, G., Weaver, J. C., Saadat, M., Bertoldi, K., & Lauder, G. V. (2018a). Hydrodynamic properties of biomimetic shark skin: Effect of denticle size and swimming speed. *Bioinspiration & Biomimetics*, *13*(5), 056014. https://doi.org/10.1088/1748-3190/aad418

Domel, A. G., Saadat, M., Weaver, J. C., Haj-Hariri, H., Bertoldi, K., & Lauder, G. V. (2018b). Shark skin-inspired designs that improve aerodynamic performance. *Journal of The Royal Society Interface*, *15*(139), 20170828. https://doi.org/10.1098/rsif.2017.0828

Donley, J. M., Sepulveda, C. A., Konstantinidis, P., Gemballa, S., & Shadwick, R. E. (2004). Convergent evolution in mechanical design of lamnid sharks and tunas [Number: 6987

Publisher: Nature Publishing Group]. *Nature*, *429*(6987), 61–65. https://doi.org/10.1038/nature02435

Du, Z., Li, H., Cao, Y., Wan, X., Xiang, Y., Lv, P., & Duan, H. (2022). Control of flow separation using biomimetic shark scales with fixed tilt angles. *Experiments in Fluids*, *63*(10), 158. https://doi.org/10.1007/s00348-022-03517-3

Du Clos, K. T., Lang, A., Devey, S., Motta, P. J., Habegger, M. L., & Gemmell, B. J. (2018). Passive bristling of mako shark scales in reversing flows. *Journal of The Royal Society Interface*, *15*(147), 20180473. https://doi.org/10.1098/rsif.2018.0473

Feld, K., Kolborg, A. N., Nyborg, C. M., Salewski, M., Steffensen, J. F., & Berg-Sørensen, K. (2019). Dermal denticles of three slowly swimming shark species: Microscopy and flow visualization. *Biomimetics*, *4*(2), 38. https://doi.org/10.3390/biomimetics4020038

Gabler-Smith, M., Wainwright, D., Wong, G., & Lauder, G. (2021). Dermal denticle diversity in sharks: Novel patterns on the interbranchial skin. *Integrative Organismal Biology*, *3*(1). https://doi.org/10.1093/iob/obab034

Gabler-Smith, M. K., & Lauder, G. V. (2022). Ridges and riblets: Shark skin surfaces versus biomimetic models. *Frontiers in Marine Science*, *9*, 975062. https://doi.org/10.3389/fmars.2022.975062

Ghimire, A., Dahl, R. B., Shen, S.-F., & Chen, P.-Y. (2024). Shark skin denticles: From morphological diversity to multi-functional adaptations and applications. *Advanced Functional Materials*, 2307121.

Han, X., & Zhang, D. (2008). Study on the micro-replication of shark skin. *Science in China Series E: Technological Sciences*, *51*(7), 890–896.

Ibrahim, M. D., Amran, S. N. A., Yunos, Y. S., Rahman, M. R. A., Mohtar, M. Z., Wong, L. K., & Zulkharnain, A. (2018). The study of drag reduction on ships inspired by simplified shark skin imitation [Publisher: Hindawi]. *Applied Bionics and Biomechanics*, *2018*, e7854321. https://doi.org/10.1155/2018/7854321

Jo, W., Kang, H. S., Choi, J., Jung, J., Hyun, J., Kwon, J., Kim, I., Lee, H., & Kim, H.-T. (2021). Light-designed shark skin-mimetic surfaces [Publisher: American Chemical Society]. *Nano Letters*, *21*(13), 5500–5507. https://doi.org/10.1021/acs.nanolett.1c00436

Lang, A., Motta, P., Habegger, M., Hueter, R., & Afroz, F. (2011). Shark skin separation control mechanisms. *Marine Technology Society Journal*, *45*(4), 208–215. https://doi.org/10.4031/MTSJ.45.4.12

Lang, A. W., Motta, P., Hidalgo, P., & Westcott, M. (2008). Bristled shark skin: A microgeometry for boundary layer control? *Bioinspiration & Biomimetics*, *3*(4), 046005. https://doi.org/10.1088/1748-3182/3/4/046005

Lang, A., Habegger, M. L., & Motta, P. (2015). Shark skin drag reduction. In B. Bhushan (Ed.), *Encyclopedia of nanotechnology* (pp. 1–8). Springer Netherlands. https://doi.org/10.1007/978-94-007-6178-0_266-2

Lang, A. W., Bradshaw, M. T., Smith, J. A., Wheelus, J. N., Motta, P. J., Habegger, M. L., & Hueter, R. E. (2014). Movable shark scales act as a passive dynamic microroughness to control flow separation. *Bioinspiration & Biomimetics*, *9*(3), 036017. https://doi.org/10.1088/1748-3182/9/3/036017

Lang, A., Bradshaw, M., Smith, J., Wheelus, J., Motta, P., Habegger, M., & Hueter, R. (2014). Movable shark scales act as a passive dynamic micro-roughness to control flow separation. *Bioinspiration and Biomimetics*, *9*(3). https://doi.org/10.1088/1748-3182/9/3/036017

Lang, A., Motta, P., Hidalgo, P., & Westcott, M. (2008). Bristled shark skin: A microgeometry for boundary layer control? *Bioinspiration and Biomimetics*, *3*(4). https://doi.org/10.1088/1748-3182/3/4/046005

Lloyd, C., Peakall, J., Burns, A., Keevil, G., Dorrell, R., Wignall, P., & Fletcher, T. (2021). Hydrodynamic efficiency in sharks: The combined role of riblets and denticles. *Bioinspiration and Biomimetics*, *16*(4). https://doi.org/10.1088/1748-3190/abf3b1

Luo, Y., Liu, Y., & Zhang, D. Y. (2015). Prediction the variation of shark scale's attack angles in swimming. *Indian Journal of Animal Research*, *49*(3), 295. https://doi.org/10.5958/0976-0555.2015.00088.6

Meyer, W., & Seegers, U. (2012). Basics of skin structure and function in elasmobranchs: A review. *Journal of Fish Biology*, *80*(5), 1940–1967. https://doi.org/10.1111/j.1095-8649.2011.03207.x

Miyazaki, M., Hirai, Y., Moriya, H., Shimomura, M., Miyauchi, A., & Liu, H. (2018). Biomimetic riblets inspired by sharkskin denticles: Digitizing, modeling and flow simulation. *Journal of Bionic Engineering*, *15*(6), 999–1011. https://doi.org/10.1007/s42235-018-0088-7

Motta, P., Habegger, M. L., Lang, A., Hueter, R., & Davis, J. (2012). Scale morphology and flexibility in the shortfin mako isurus oxyrinchus and the blacktip shark carcharhinus limbatus. *Journal of Morphology*, *273*(10), 1096–1110. https://doi.org/10.1002/jmor.20047

Naresh, M. D., Arumugam, V., & Sanjeevi, R. (1997). Mechanical behaviour of shark skin. *Journal of Biosciences*, *22*(4), 431–437. https://doi.org/10.1007/BF02703189

Oeffner, J., & Lauder, G. V. (2012). The hydrodynamic function of shark skin and two biomimetic applications. *Journal of Experimental Biology*, *215*(5), 785–795. https://doi.org/10.1242/jeb.063040

Page, M. J., McKenzie, J. E., Bossuyt, P. M., Boutron, I., Hoffmann, T. C., Mulrow, C. D., Shamseer, L., Tetzlaff, J. M., Akl, E. A., Brennan, S. E., et al. (2021). The prisma 2020 statement: An updated guideline for reporting systematic reviews. *Bmj*, *372*.

Patricia, F.-W., Guzman, D., Iñigo, B., Urtzi, I., Maria, B., & Manu, S. (2019). Morphological characterization and hydrodynamic behavior of shortfin mako shark (isurus oxyrinchus) dorsal fin denticles. *Journal of Bionic Engineering*, *16*(4), 730–741. https://doi.org/10.1007/s42235-019-0059-7

Peng, Y. L., Lin, C. G., & Wang, L. (2009). The preliminary study on antifouling mechanism of shark skin. *Advanced Materials Research*, *79*, 977–980.

Popp, M., White, C., Bernal, D., Wainwright, D., & Lauder, G. (2020). The denticle surface of thresher shark tails: Three-dimensional structure and comparison to other pelagic species. *Journal of Morphology*, *281*(8), 938–955. https://doi.org/10.1002/jmor.21222

Pu, X., Li, G., & Liu, Y. (2016). Progress and perspective of studies on biomimetic shark skin drag reduction. *ChemBioEng Reviews*, *3*(1), 26–40. https://doi.org/10.1002/cben.201500011

Reif, W. (1978). Protective and hydrodynamic function of the dermal skeleton of elasmobranchs.

Reif, W., & Dinkelacker, A. (1982). Hydrodynamics of the squamation in fast swimming sharks. *Neues Jahrbuch für Geologie und Paläontologie-Abhandlungen*, *164*(1-2), 184–187.

Runchal, A. K., & Rao, M. M. (2020). Cfd of the future: Year 2025 and beyond. *50 Years of CFD in Engineering Sciences: A Commemorative Volume in Memory of D. Brian Spalding*, 779–795.

Santos, L. M., Lang, A., Wahidi, R., Bonacci, A., Gautam, S., Devey, S., & Parsons, J. (2021). Passive separation control of shortfin mako shark skin in a turbulent boundary layer. *Experimental Thermal and Fluid Science*, *128*, 110433.

Southall, E. J., & Sims, D. W. (2003). Shark skin: A function in feeding. *Proceedings of the Royal Society of London. Series B: Biological Sciences*, *270*. https://doi.org/10.1098/rsbl.2003.0006

Wainwright, S. A., Vosburgh, F., & Hebrank, J. H. (1978). Shark skin: Function in locomotion. *Science*, *202*(4369), 747–749. https://doi.org/10.1126/science.202.4369.747

Wen, J., Prawel, D., & Li, Y. V. (2023). A study on the mechanical and antimicrobial properties of biomimetic shark skin fabrics with different denticle size via 3d printing technology [Publisher: IOP Publishing]. *Physica Scripta*, *98*(3), 035031. https://doi.org/10.1088/1402-4896/acbc58

Wen, L., Weaver, J. C., & Lauder, G. V. (2014). Biomimetic shark skin: Design, fabrication and hydrodynamic function. *Journal of Experimental Biology*, *217*(10), 1656–1666. https://doi.org/10.1242/jeb.097097

Wen, L., Weaver, J. C., Thornycroft, P. J. M., & Lauder, G. V. (2015). Hydrodynamic function of biomimetic shark skin: Effect of denticle pattern and spacing [Publisher: IOP Publishing]. *Bioinspiration & Biomimetics*, *10*(6), 066010. https://doi.org/10.1088/1748-3190/10/6/066010

Zhang, C., Gao, M., Liu, G., Zheng, Y., Xue, C., & Shen, C. (2022). Relationship between skin scales and the main flow field around the shortfin mako shark isurus oxyrinchus. *Frontiers in Bioengineering and Biotechnology*, *10*. https://doi.org/10.3389/fbioe.2022.742437

Zhang, D.-y., Luo, Y.-h., Li, X., & Chen, H.-w. (2011). Numerical simulation and experimental study of drag-reducing surface of a real shark skin. *Journal of Hydrodynamics*, *23*(2), 204–211. https://doi.org/10.1016/S1001-6058(10)60105-9

Zhao, D., Tian, Q., Wang, M., & Jin, Y. (2014). Study on the hydrophobic property of shark-skin-inspired micro-riblets. *Journal of Bionic Engineering*, *11*(2), 296–302.